Petroleum Science 23 (2026) 393–421

Contents lists available at ScienceDirect

Petroleum Science

journal homepage: www.keaipublishing.com/en/journals/petroleum-science

Formulation, stability, and synergistic characteristics of diesel-in-water Pickering emulsions stabilized by titanium carbide ($Ti_3C_2T_x$) MXene and Tween 40

Nansee S.K. Abu Zaid [a], Aaminah Johar [a], Mustafa S. Nasser [a,b,*], Khaled A. Mahmoud [c], Sagheer A. Onaizi [d,e,**]

[a] Gas Processing Center, College of Engineering, Qatar University, P.O. Box 2713, Doha, Qatar
[b] Department of Chemical Engineering, College of Engineering, Qatar University, P.O. Box 2713, Doha, Qatar
[c] Qatar Environment and Energy Research Institute (QEERI), Hamad Bin Khalifa University, Qatar Foundation, P.O. Box 34110, Doha, Qatar
[d] Department of Chemical Engineering, King Fahd University of Petroleum and Minerals, Dhahran 31216, Saudi Arabia
[e] Interdisciplinary Research Center for Hydrogen Technologies and Carbon Management, King Fahd University of Petroleum and Minerals, Dhahran 31216, Saudi Arabia

ARTICLE INFO

Article history:
Received 22 March 2025
Received in revised form
6 October 2025
Accepted 14 October 2025
Available online 24 October 2025

Edited by Yan-Hua Sun

Keywords:
Titanium carbide ($Ti_3C_2T_x$) MXene nanosheets
Oil-in-water (O/W) Pickering emulsions
Tween 40 chemical surfactant
Pickering emulsion characteristics
Emulsion stability
Emulsion rheology

ABSTRACT

Enhanced oil recovery (EOR) operations increasingly depend on emulsion-based formulations that exhibit long-term stability under reservoir conditions while minimizing surfactant dosage. In this context, hybrid systems combining nanoparticles and surfactants offer a promising route to achieving both interfacial stability and formulation efficiency. Among potential nanoparticle candidates, $Ti_3C_2T_x$ MXene exhibits high surface area and interfacial activity. However, its application in diesel-in-water Pickering emulsions under EOR-relevant conditions has not been explored. Challenges such as high hydrophilicity and strong electrostatic repulsion have limited the use of unmodified MXene as a standalone stabilizer in colloidal systems. To address this limitation, diesel-in-water Pickering emulsions were formulated using DL-$Ti_3C_2T_x$ MXene combined with Tween 40 (0.5 wt%) and antifoam (0.15 wt%), aiming to investigate their synergistic stabilization behavior across MXene concentrations ranging from 0.1 to 1.5 wt%. The MXene-only system exhibited complete and immediate phase separation, whereas the hybrid emulsions demonstrated markedly enhanced stability, with no phase separation observed at 0.1 and 0.5 wt% after 24 h. A concentration-dependent trend was evident. At lower MXene contents, interfacial adsorption improved, and droplet sizes remained small and uniform. At higher concentrations ($\geq$ 1.0 wt%), aggregation increased, and demulsification became more pronounced. Interfacial tension decreased steadily with increasing MXene content, reaching 0.86 mN/m at 1.5 wt%, while zeta potential remained strongly negative (-47.7 mV at 0.5 wt%), indicating sufficient electrostatic repulsion. Rheological analysis revealed a transition to shear-thinning behavior at higher MXene contents, confirming the formation of internal network structures. Compared to other reported systems based on silica (SiO_2), zinc oxide (ZnO), or functionalized MXenes, the MXene-Tween 40 formulation achieved superior short- and long-term emulsion stability without requiring surface modification or external stimuli. To the best of our knowledge, this is the first study to report the successful stabilization of diesel-in-water Pickering emulsions using unmodified $Ti_3C_2T_x$ MXene. These findings highlight the synergistic interaction between MXene and Tween 40 and present a robust, surfactant-lean formulation suitable for oilfield applications.

1. Introduction

Primary and secondary crude oil recovery typically leave up to 70% of the original oil in place, immobilized by capillary forces within the reservoir rock (Ibrahim Youssif and Saleh, 2024).

* Corresponding author.
** Corresponding author.
E-mail addresses: m.nasser@qu.edu.qa (M.S. Nasser), onaizi@kfupm.edu.sa (S.A. Onaizi).
Peer review under the responsibility of China University of Petroleum (Beijing).

https://doi.org/10.1016/j.petsci.2025.10.013

Chemical enhanced oil recovery (cEOR) strategies, including surfactant, polymer, and alkali flooding, aim to reduce interfacial tension (IFT), alter wettability, and improve fluid mobility. However, their effectiveness is often limited by polymer degradation, surfactant adsorption, and corrosion issues (Habib et al., 2024). Among cEOR techniques, emulsion flooding has shown notable success, where oil-in-water (O/W) or water-in-oil (W/O) emulsions can mobilize trapped oil through porous media (Adil and Onaizi, 2022). When solid nanoparticles (NPs) are used as stabilizers, the resulting systems are referred to as Pickering emulsions (Goodarzi and Zendehboudi, 2019). These particles irreversibly adsorb at oil–water interfaces, forming rigid interfacial layers that resist coalescence and improve stability under harsh salinity, temperature, and pH conditions (Pinto et al., 2025). NPs can also enhance sweep efficiency by increasing viscosity, altering wettability, and preventing asphaltene precipitation or pore plugging (Iravani et al., 2023). A wide range of materials including SiO_2, cellulose, carbon nanotubes, and metal oxides have been explored for such applications (de Carvalho-Guimarães et al., 2022). Recent studies confirm that NP-stabilized emulsions outperform conventional chemical flooding systems in terms of oil recovery and pressure maintenance (Pinto et al., 2025; Saha and Phukan, 2025; Zhao et al., 2024b).

A growing strategy in EOR involves hybrid-stabilized emulsions, where NPs are combined with surfactants to enhance performance (Jia et al., 2022). Surfactants improve nanoparticle dispersion and interfacial adsorption, while the nanoparticles provide mechanical rigidity and reduce sensitivity to salinity and temperature (Li et al., 2024). This synergy lowers surfactant demand, reducing cost and environmental impact (Khezerloo-ye Aghdam et al., 2024). For instance, Paryoto et al. (2023) studied Fe_3O_4 nanoparticles combined with a binary surfactant mixture of anionic S11 and amphoteric S20, achieving enhanced droplet stability and wettability alteration compared to surfactant-only systems under high salinity and temperature in EOR settings. Similarly, Rezvani et al. (2024) utilized epoxysilane-functionalized SiO_2 NPs with two surfactant systems: a zwitterionic alkyl hydroxysultaine (AHS) and a zwitterionic-non-ionic (ZN) blend. The AHS-based formulation yielded more stable emulsions, highlighting the role of NP-surfactant compatibility in oil recovery. Gazem et al. (2025a) developed ternary low-salinity EOR formulations using ZnO NPs, rhamnolipid or sophorolipid biosurfactants, and xanthan gum, which improved IFT reduction, emulsion stability, and viscosity compared to binary or individual components. In a related study, Tliba et al. (2025) synthesized SiO_2 NPs functionalized with sodium olefin sulfonate (SOS) and ammonium lauryl sulfate (ALS), achieving ultra-low IFT, wettability alteration, and stable O/W emulsions that outperformed both unmodified SiO_2 and single surfactant systems. Collectively, these findings confirm that well-designed NP-surfactant systems consistently outperform individual components. Such systems not only improve emulsion robustness but also enhance sweep efficiency and reduce surfactant adsorption in porous media, making them promising for field deployment (Pei et al., 2024; Xu et al., 2022).

Among emerging nanomaterials, MXenes (e.g., $Ti_3C_2T_x$) have attracted attention for their high surface area, tunable surface chemistry, and strong interfacial activity (Salim et al., 2019). Their two-dimensional (2D) sheet-like morphology and multilayered structure allow dense coverage at fluid interfaces, which is highly desirable for stabilizing emulsions (Ma et al., 2024). However, these advantages are counteracted by their high hydrophilicity, caused by surface terminations such as –OH, –F, and =O, which hinder spontaneous adsorption at oil–water interfaces and disrupt amphiphilic balance (Cain et al., 2019). As a result, unmodified MXenes often fail to stabilize oil-rich emulsions without prior chemical modification, limiting their use in surfactant-lean or additive-free systems. Although several studies have focused on tailoring MXene wettability through surface functionalization, limited attention has been given to leveraging their intrinsic architecture and properties, to improve emulsion stability under low-surfactant conditions.

MXene-based Pickering emulsions have been reported primarily for non-oilfield applications. For example, Yang et al. (2025a) used sodium carboxymethyl cellulose (CMC)-modified $Ti_3C_2T_x$ to stabilize polydimethylsiloxane (PDMS) emulsions for sensor aerogels. Ma et al. (2024) applied dual modifications with polydopamine and fluorosilane to tailor $Ti_3C_2T_x$ amphiphilicity for stabilizing methyl methacrylate (MMA) and butyl acrylate (BA) emulsions. Fan et al. (2022) developed water-in-ionic-liquid Pickering emulsions for porous monoliths in solar evaporation applications. Wang et al. (2025) created cottonseed oil-based Pickering emulsions using β-cyclodextrin and Ti_3C_2 MXene as a green nano-cutting fluid, which enhanced thermal conductivity and lubrication. Cao et al. (2021) used $Ti_3C_2T_x$-stabilized emulsions to fabricate polymer composites with excellent electrical conductivity, electromagnetic interference shielding for flexible electronics. Thota et al. (2025) prepared a superhydrophilic, MXene-based nanofibrous membrane for oil–water separation, achieving 99% separation efficiency and excellent reusability in emulsion filtration. While these studies demonstrate the versatility of MXene-based emulsions, they primarily focus on coatings, composites, electronics, or environmental uses. To date, to the best of our knowledge, no study has explored the use of pristine $Ti_3C_2T_x$ MXene in Pickering emulsions for enhanced oil recovery or related oilfield applications. Likewise, the synergistic interaction between unmodified MXene and surfactants remains unexamined in such systems. The only related work is that of He et al. (2024), who grafted polyethylene glycol (PEG) onto carboxylated $Ti_3C_2T_x$ and combined it with sodium dodecylbenzenesulfonate (SDBS). Their modified formulation improved emulsion viscosity and stability under different salinity, pH, and temperature conditions. However, their system required chemical modification and relatively high surfactant loading, which may not be ideal for surfactant-lean or additive-minimized formulations. In contrast, this study proposes a distinct formulation strategy that utilizes the inherent structural characteristics of unmodified $Ti_3C_2T_x$ MXene to enable interfacial anchoring and improve emulsion stability in diesel-in-water systems designed for EOR. Rather than relying on surface functionalization or high surfactant content, the formulation leverages MXene's architecture to achieve physical stabilization in synergy with a minimal amount of non-ionic surfactant.

Despite recent progress in emulsion-based EOR, the development of stable diesel-in-water Pickering emulsions using unmodified MXene has not been reported in the literature. Although $Ti_3C_2T_x$ MXene nanosheets and the non-ionic surfactant Tween 40 have each shown promise in stabilizing emulsions, their combined use and the resulting synergistic effects remain unexplored. In particular, no studies have investigated the interfacial behavior, dispersion characteristics, or structural stabilization mechanisms of unmodified $Ti_3C_2T_x$ MXene in the presence of a minimal surfactant under oilfield-relevant conditions. This study addresses these gaps by formulating diesel-in-water Pickering emulsions using varying concentrations of unmodified MXene (0.1–1.5 wt%) in combination with Tween 40 (0.5 wt%). Comprehensive characterization was performed, including zeta potential, droplet size distribution, interfacial tension, optical microscopy, kinetic stability, and rheological behavior under varying temperatures and shear rates. The results demonstrate that the sheet-like structure, and surface chemistry of MXene enable strong interfacial anchoring and multilayer tiling when supported by a minimal

amount of surfactant. This structural advantage facilitates the formation of stable droplets and reduces surfactant demand. To the best of our knowledge, this is the first report on diesel-in-water Pickering emulsions stabilized by unmodified MXene and Tween 40 for oilfield applications. The findings provide insights into the structure-stability relationship of 2D material-based system and provide a practical foundation for developing robust, surfactant-lean systems for enhanced oil recovery.

2. Experimental methods

2.1. Materials

Delaminated $Ti_3C_2T_x$ MXene was synthesized using the Ti_3AlC_2 MAX phase obtained from Y-Carbon Ltd., hydrochloric acid (HCl, Merck), and lithium fluoride (LiF, 99.0%, Sigma-Aldrich). Pickering emulsions were prepared using DL-$Ti_3C_2T_x$ nanosheets and Tween 40 (polyoxyethylene sorbitan monopalmitate, Sigma-Aldrich) as stabilizers. A commercial antifoaming agent (AMEREL® 1500) was added to prevent excessive foam formation during emulsification. Diesel, used as the oil phase, was sourced locally (WOQOD, Qatar), and deionized water was supplied by a Milli-Q purification system. The density of diesel was measured as 0.8282 g/mL at 25±0.5 °C using an Anton Paar DMA 5000 M densitometer. All materials were used as received without further purification.

2.2. Synthesis of DL-$Ti_3C_2T_x$ MXene

Delaminated $Ti_3C_2T_x$ MXene nanosheets (DL-$Ti_3C_2T_x$) were synthesized via selective etching of the Ti_3AlC_2 MAX phase using a LiF/HCl solution, following the method reported by Rasool et al. (2016) with minor modifications. The synthesis procedure is illustrated in Fig. 1. A solution was first prepared by dissolving 1.6 g of LiF in 14.8 mL of 9 mol/L HCl in a Teflon jar. Subsequently, 1 g of Ti_3AlC_2 MAX phase was gradually added to the solution under continuous stirring at room temperature. The mixture was stirred for 24 h to complete the etching reaction. Following etching, the resulting suspension was centrifuged and washed repeatedly with deionized water until the supernatant reached a pH of approximately 5.5. Delamination was initiated by purging the suspension

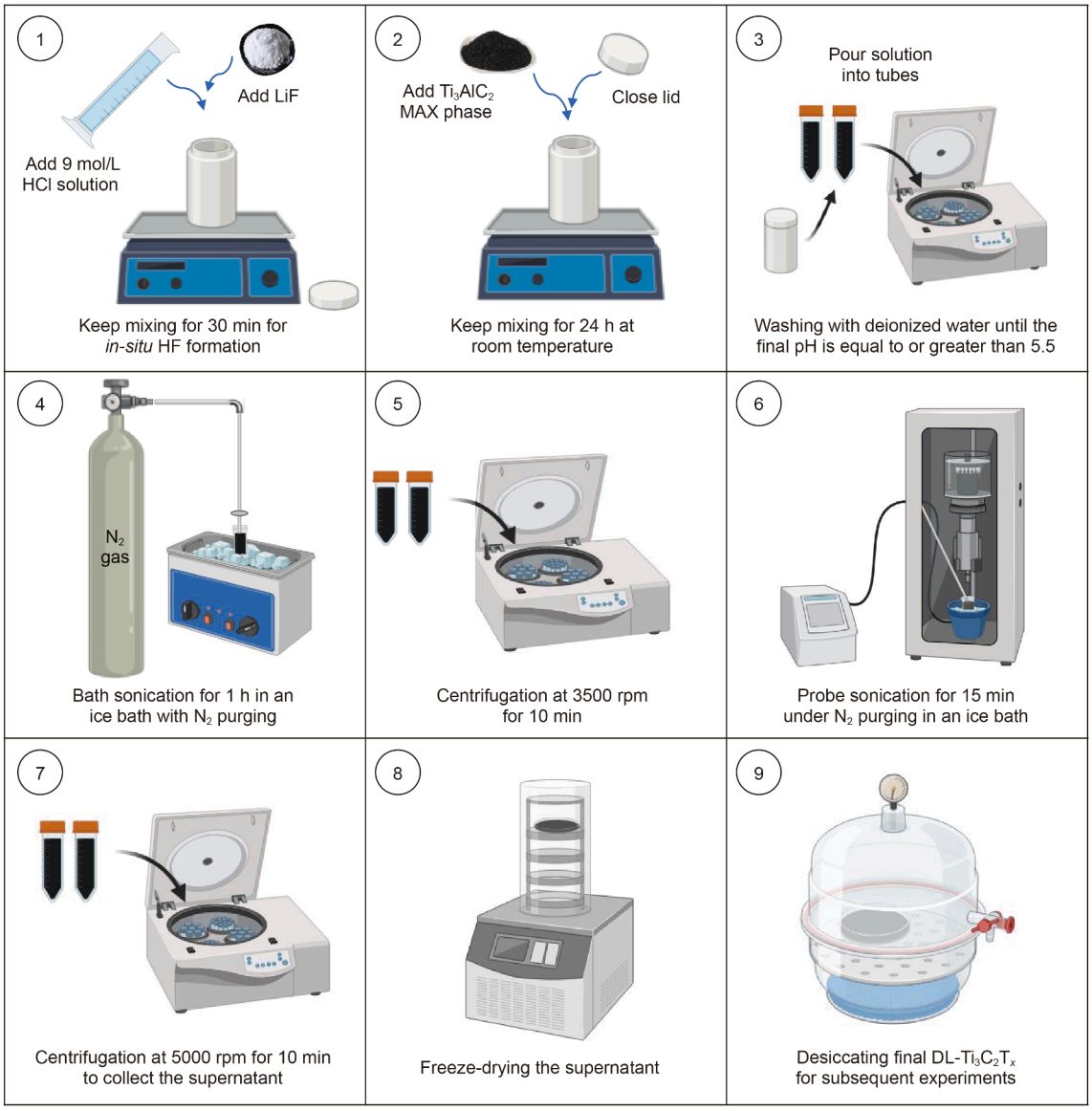

Fig. 1. Synthesis of DL-$Ti_3C_2T_x$ MXene nanosheets.

with nitrogen gas (N_2), followed by bath sonication for 1 h in an ice bath to regulate temperature. This process facilitated the exfoliation of $Ti_3C_2T_x$ nanosheets from the multilayered MXene. The suspension was then centrifuged at 3500 rpm for 10 min, and the supernatant containing delaminated nanosheets was collected. To recover additional delaminated MXene, the remaining sediment was re-dispersed in deionized water, purged with N_2, and subjected to probe sonication for 15 min in an ice bath. The suspension was centrifuged again at 5000 rpm for 10 min, and the supernatant was collected. This process was repeated until no significant amount of multilayered MXene remained. The final DL-$Ti_3C_2T_x$ nanosheets were recovered from the combined supernatants by freeze-drying and stored in a desiccator for further use.

2.3. DL-$Ti_3C_2T_x$ MXene characterization

The crystallographic structure of the DL-$Ti_3C_2T_x$ MXene nanosheets was analyzed using X-ray diffraction (XRD, Bruker AXS D4 Endeavour™, Germany) with Cu-Kα radiation ($\lambda = 1.5444$ Å). A continuous scan was performed over a 2θ range of 5°–65°, using a step size of 0.013° and a scan speed of 1 °/min. The measurements were conducted at 45 kV and 40 mA. Surface morphology and elemental composition were examined using a field emission scanning electron microscope (FE-SEM, Nova Nano SEM 450, ThermoFisher, USA) operating at an accelerating voltage of 10 kV. Energy-dispersive X-ray spectroscopy (EDS) was used in conjunction with SEM to confirm the elemental distribution of the nanosheets. High-resolution transmission electron microscopy (HRTEM, TECNAI G2 20 S-TWIN, FEI, USA) was employed to further investigate the internal morphology and layered structure of the synthesized MXene. The HRTEM analysis was carried out at an accelerating voltage of 200 kV.

2.4. Preparation of DL-$Ti_3C_2T_x$ Pickering emulsions

Pickering emulsions containing various concentrations of DL-$Ti_3C_2T_x$ nanosheets (0.0, 0.1, 0.5, 1.0, and 1.5 wt%) were prepared following a modified method based on previously reported protocols (Abu Zaid et al., 2025). The aqueous phase was first prepared by dispersing the required amount of DL-$Ti_3C_2T_x$ in deionized water, followed by probe sonication in an ice bath (20 min, 70% amplitude, 20 kHz, 15 s on/5 s off) to ensure homogeneous dispersion and exfoliation of the nanosheets. Several surfactants were preliminarily screened for compatibility with MXene. Tween 40 was selected based on its superior synergy and emulsion stability in the presence of DL-$Ti_3C_2T_x$. As a non-ionic surfactant, Tween 40 exhibits minimal adsorption onto reservoir rock surfaces, which is a critical advantage in EOR operations since it reduces chemical loss and improves process economics (Abu Zaid et al., 2025). The concentration of Tween 40 was optimized to achieve stable emulsions while minimizing usage. Screening tests identified 0.5 wt% Tween 40 as the minimum required to form robust emulsions with MXene. Although higher concentrations (e.g., 1.0 wt%) improved stability, they were considered excessive for practical EOR scenarios. Lower concentrations (0.1–0.3 wt%) were insufficient for stable emulsion formation. To control foaming during sonication and mixing, 0.15 wt% AMEREL® 1500 antifoam was included in all formulations. This dosage was found to be the minimum effective concentration. Compatibility between Tween 40 and AMEREL® 1500 was confirmed by the absence of precipitation or emulsion destabilization in all trials. After initial dispersion of the DL-$Ti_3C_2T_x$ nanosheets, Tween 40 (0.5 wt%) and AMEREL® 1500 (0.15 wt%) were added and stirred at 600 rpm for 15 min to achieve uniform mixing. The mixture then underwent a second sonication step (5 min in an ice bath) to further improve dispersion stability. The oil phase (diesel) was introduced gradually into the aqueous phase at a 1:1 volume ratio over 10 min while stirring at 600 rpm. Following complete addition, the emulsion was stirred for an additional 15 min to enhance mixing, followed by a final ultrasonication step (10 min in an ice bath) to improve droplet uniformity and ensure long-term emulsion stability. Three types of systems were prepared for comparison: (i) MXene-only emulsions (no surfactant or antifoam), (ii) control emulsions containing Tween 40 and antifoam (no MXene), and (iii) hybrid emulsions combining DL-$Ti_3C_2T_x$ nanosheets, Tween 40, and antifoam. The type of emulsion was confirmed via a droplet test, in which a small amount of the freshly prepared emulsion was placed in both water and diesel. The emulsion dispersed in water but remained separate in diesel, confirming an O/W emulsion. A schematic illustration of the hybrid stabilization mechanism in the MXene-Tween 40-stabilized system is provided in Fig. 2. DL-$Ti_3C_2T_x$ nanosheets adsorb at the oil–water interface of diesel droplets, forming a rigid interfacial layer, while Tween 40 provides a hydrated steric barrier that enhances droplet stability and prevents coalescence.

2.5. Characterization of Pickering emulsions

2.5.1. Evaluation of kinetic stability

The long-term kinetic stability of DL-$Ti_3C_2T_x$-based Pickering emulsions was assessed by monitoring phase separation over

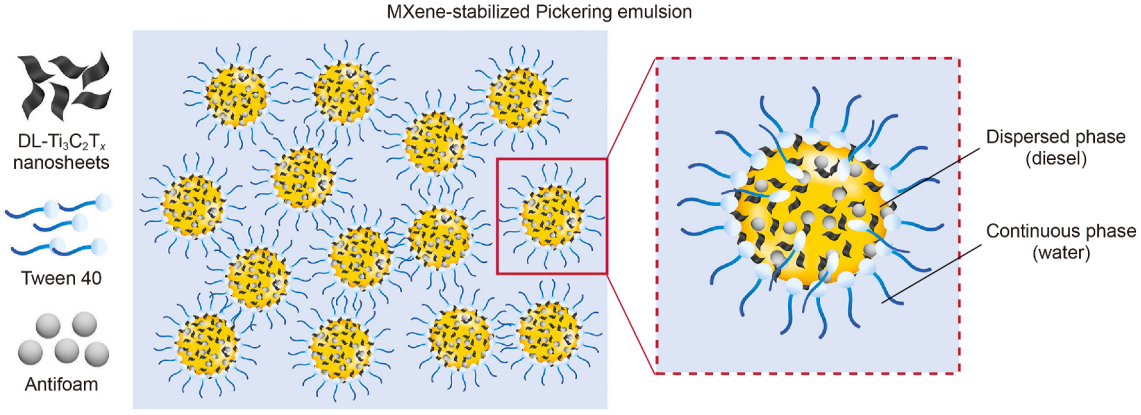

Fig. 2. Schematic illustration of MXene-Tween 40-stabilized diesel-in-water Pickering emulsions. The figure depicts the structural arrangement of DL-$Ti_3C_2T_x$ nanosheets, Tween 40, and antifoam at the oil–water interface, forming a stabilized emulsion system with dispersed diesel droplets (yellow) in a continuous water phase (blue).

time. Immediately after emulsification, each sample was transferred to a graduated cylinder, sealed with parafilm, and stored at ambient temperature for 30 d. During this period, emulsions were visually monitored at regular intervals, and the volume of separated water and/or oil was recorded. The demulsification index (DI) was calculated using the following equation:

$$DI = \frac{V_t}{V_0} \times 100\% \quad (1)$$

where V_t and V_0 represent the volume of water or diesel separated from the Pickering emulsion at time t and the initial volume of water or diesel oil in the Pickering emulsion, respectively.

2.5.2. Optical microscopy

A binocular microscope (OPTIKA B-500, OPTIKA S.r.l., Ponteranica, Italy) equipped with an integrated camera was used to examine the microstructure of the Pickering emulsions. A small volume of emulsion was placed on a microscope slide, covered with a coverslip, and observed under 40× magnification. The obtained images provided useful insights into the uniformity and distribution of the droplets within the emulsion.

2.5.3. Zeta potential measurements

Zeta potential measurements were performed using a Zetasizer ZEN3600 (Malvern Instruments Ltd., UK) immediately after sonication. To reduce multiple scattering, samples were diluted with deionized water and loaded into Malvern DTS1070 disposable folded capillary cells. Measurements were conducted at 25 °C after a 120 s equilibration period. Each sample was measured in triplicate, and the average value was reported.

2.5.4. Droplet size measurements

Droplet size measurements of Pickering emulsions were performed using dynamic light scattering (DLS) on a Zetasizer ZEN3600 (Malvern Instruments Ltd.). To minimize the influence of emulsion aging, this analysis was conducted immediately after sonication. The Pickering emulsion sample was placed in a ZEN0040 disposable plastic micro cuvette, and measurements were taken using a non-invasive backscatter (NIBS) detector positioned at a 173° angle. The sample was allowed to equilibrate at 25 °C for 120 s to ensure stability during measurements. Each measurement was repeated three times, and the mean droplet size was calculated by averaging these values, providing a dependable assessment of the emulsion properties.

2.5.5. Dynamic IFT measurements

A drop-shape analyzer (DSA100S, KRÜSS, Germany) was used to evaluate the dynamic IFT of Pickering emulsions stabilized by DL-$Ti_3C_2T_x$ nanosheets. For each sample, a droplet of emulsion was gently formed at the tip of a stainless-steel needle in a quartz cuvette filled with diesel. The measurement was conducted at a controlled temperature of 25 °C over a 1 h period. The droplet shape was captured continuously by a high-resolution camera, and its contour was analyzed using the Young–Laplace equation to calculate the time-resolved IFT values.

2.5.6. Rheological measurements

The flow behavior of the emulsions was characterized using a Modular Compact Rheometer (MCR 302, Anton Paar Ltd., Graz, Austria) with a CC27 cup-and-bob geometry. Prior to testing, the bob-cup gap was adjusted to 1 mm, and a 5 min equilibrium period was allowed. Freshly prepared samples were used in all tests to avoid effects of emulsion aging. The rheological analysis included frequency sweep, temperature ramp, and flow curve tests to evaluate viscoelastic and thermal responses.

2.5.6.1. Dynamic rheological behavior. The dynamic properties of the Pickering emulsions were evaluated using frequency sweep tests to capture both the elastic (G') and viscous (G'') responses. Measurements were taken over a frequency range of 1–600 rad/s, at three distinct temperatures: 25, 45, and 65 °C, to observe how temperature variations influence the rheological behavior. These tests were performed as part of the rheological characterization to provide a comprehensive understanding of the emulsions' flow properties.

2.5.6.2. Thermal behavior. To explore the thermal stability of the formulated Pickering emulsions, temperature ramp tests were carried out. The tests involved a systematic temperature change, starting from 25 °C, increasing gradually up to 80 °C, and then cooling back to 25 °C. During these tests, the viscosity was continuously monitored to observe how temperature variations impact the stability and flow characteristics of Pickering emulsions. Three different flow models were used to regress and interpret the results: the Ostwald–de Waele, the Bingham, and the Herschel–Bulkley models, as respectively represented by the following equations:

$$\tau = k_{OW} \cdot \gamma^n \quad (2)$$

$$\tau = \tau_0 + \eta_B \cdot \gamma \quad (3)$$

$$\tau = \tau_0 + K_{HB} \cdot \gamma^n \quad (4)$$

where τ is the shear stress, Pa; γ is the shear rate, s^{-1}; k_{OW} and K_{HB} are the consistency indices, Pa·s^n; η_B is the Bingham viscosity, Pa·s; and τ_0 is the yield stress, Pa.

Each model provides different perspectives on emulsion flow behavior, such as shear-thinning, yield stress, or plastic viscosity (Frigaard et al., 2017; Husin et al., 2018).

2.5.6.3. Flow curve tests. Flow curve tests were conducted to assess viscosity changes across a range of shear rates (1–600 s^{-1}) at three temperatures: 25, 45, and 65 °C. The tests aimed to identify how the Pickering emulsions respond to varying shearing and thermal conditions. Some formulations displayed a shear-thinning behavior, while others showed a Newtonian or nearly constant viscosity profile, depending on their compositions and structural characteristics.

3. Results and discussion

3.1. Characterization of DL-$Ti_3C_2T_x$ MXene

To gain insights into the elemental composition, morphology, crystallinity, and surface chemistry of the synthesized DL-$Ti_3C_2T_x$ MXene, the samples were characterized using SEM, TEM, SAED, EDS, and XRD; the results are presented in Fig. 3. The SEM images (Fig. 3(a)–(c)) illustrate the transformation of DL-$Ti_3C_2T_x$ MXene nanosheets into well-defined 2D layers, confirming successful exfoliation (Gong et al., 2022). TEM analysis (Fig. 3(d)) further reveals the delaminated nanosheets at a larger scale, highlighting a clear layered structure. A highly magnified TEM image (Fig. 3(e)) focuses on the edge of a single nanosheet, showing a distinct 120° angle, which is characteristic of the hexagonal symmetry of the $Ti_3C_2T_x$ lattice. This structural feature reflects an ordered atomic arrangement and high crystallinity. The SAED pattern (Fig. 3(f)) displays clear diffraction rings corresponding to the (006), (103),

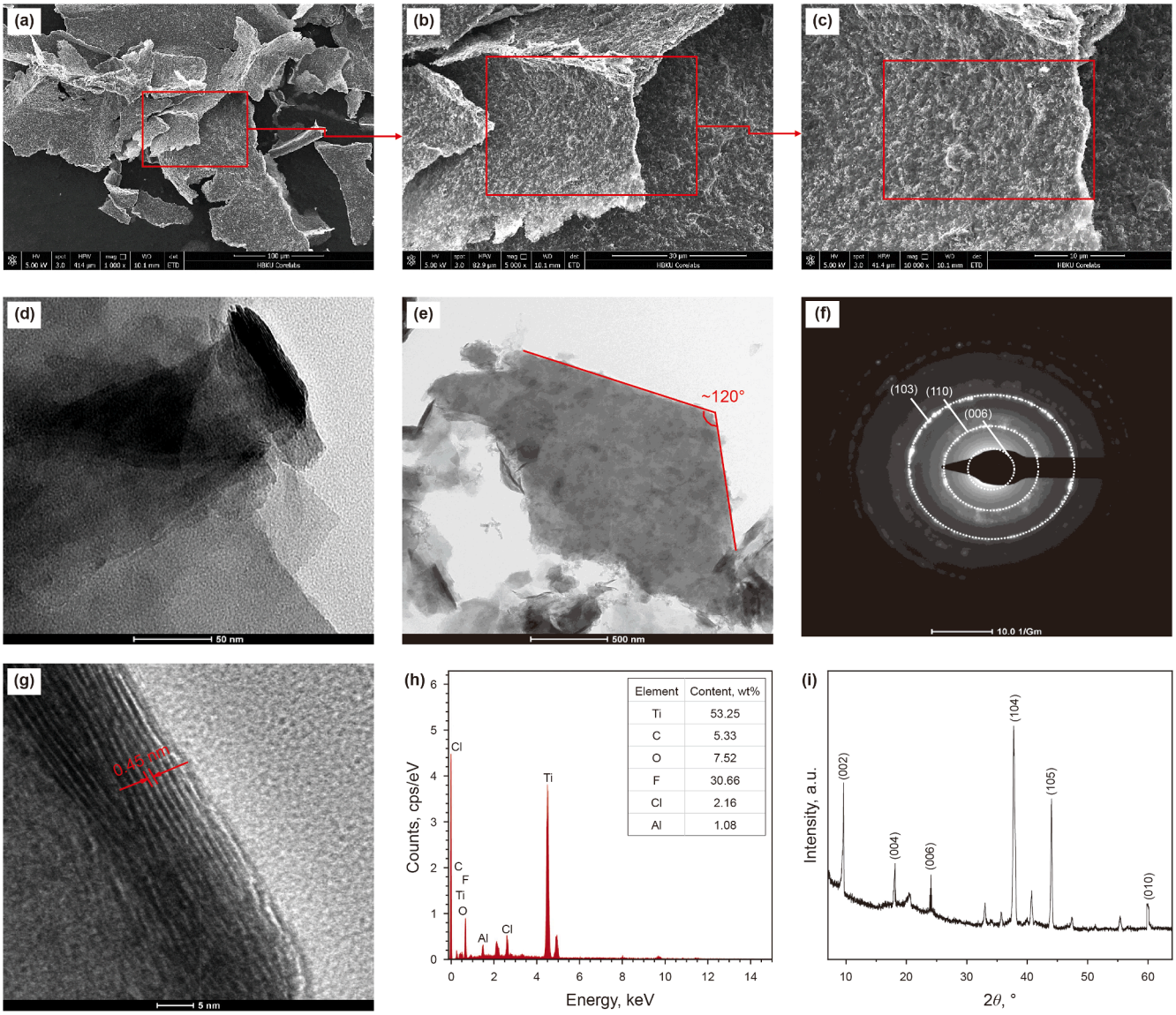

Fig. 3. (**a**)–(**c**) SEM images showing the 2D layered structure of DL-$Ti_3C_2T_x$ MXene nanosheets. (**d**) TEM image displaying the morphology. (**e**) Magnified TEM image showing a single nanosheet with a distinct 120° edge angle. (**f**) SAED pattern indicating a polycrystalline structure. (**g**) HRTEM image showing ultrathin stacking layers with ~0.45 nm spacing. (**h**) EDS analysis confirming elemental composition. (**i**) XRD pattern with characteristic peaks of the synthesized $Ti_3C_2T_x$ phase.

and (110) planes, confirming the retention of the $Ti_3C_2T_x$ crystal structure after exfoliation and indicating its polycrystalline nature. The HRTEM image (Fig. 3(g)) provides additional evidence of successful exfoliation, revealing ultrathin stacking with visible lattice fringes of approximately 0.45 nm. This morphology enhances the surface area, which is advantageous for interfacial applications. EDS analysis (Fig. 3(h)) confirms that the nanosheets are primarily composed of Ti and C, supporting the successful removal of Al from the MAX phase. The presence of surface terminations such as =O and –F is attributed to the etching process using LiF/HCl (Yan et al., 2019). The XRD pattern (Fig. 3(i)) displays well-defined peaks characteristic of the DL-$Ti_3C_2T_x$ phase. A strong peak at 6.5° corresponds to the (002) plane, indicating the layered structure and expanded interlayer spacing compared to the parent MAX phase (Ali et al., 2022). Additional reflections at 18.08°, 24°, and 30.10°, assigned to the (004), (006), and (010) planes, respectively, support the ordered stacking of the nanosheets. Peaks observed at 38.5° and 43.40° correspond to the (104) and (105) planes, while a high-angle reflection at 60.16° is attributed to the (110) plane. These features confirm the preservation of the in-plane titanium carbide structure following etching (Wang et al., 2023). Notably, the shift of the (002) peak from its original position near 9° in the MAX phase to 6.5° in the MXene sample indicates the removal of the Al layer and successful delamination, consistent with previous reports (Alhabeb et al., 2017; Ali et al., 2022; Srinivasan et al., 2022; Wang et al., 2023).

3.2. Evaluation of Pickering emulsion formation and stability

2D nanomaterials such as $Ti_3C_2T_x$ MXene have attracted significant attention as Pickering emulsion stabilizers due to their high aspect ratio and large interfacial contact area (Natalya et al., 2022). However, preliminary trials in this study confirm that unmodified MXene is ineffective for stabilizing diesel-in-water emulsions. Emulsions prepared with MXene alone showed immediate and complete phase separation, consistent with previous

reports (Cain et al., 2019; Creighton et al., 2014; Gao et al., 2020; Gonzalez Ortiz et al., 2019; Natalya et al., 2022; Salim et al., 2019; Shah et al., 2020; Taherpoor and Farzad, 2025; Yang et al., 2025a). This instability is attributed to the strong hydrophilicity and electrostatic repulsion of MXene nanosheets, as well as the absence of amphiphilic balance necessary for persistent interfacial adsorption (Creighton et al., 2014; Gao et al., 2020; Gonzalez Ortiz et al., 2019; Natalya et al., 2022; Shah et al., 2020). The presence of dense surface terminations (–OH, –F, =O) further reduces the water contact angle (29.55°–41.55°) and promotes hydrogen bonding with water molecules, favoring dispersion in the aqueous phase rather than adsorption at the oil–water interface (Han et al., 2017; Salim et al., 2019; Zhou et al., 2021).

To overcome these limitations and harness potential synergistic effects between nanoparticle and surfactant stabilizers, three emulsion systems were systematically evaluated: (i) MXene-only, (ii) a control system containing Tween 40 (0.5 wt%) and antifoam (0.15 wt%), and (iii) hybrid emulsions comprising both MXene (0.1–1.5 wt%) and Tween 40 with antifoam. Both short-term and long-term stabilities were assessed. The MXene-only system displayed immediate and complete phase separation, confirming the inadequacy of unmodified MXene as a sole stabilizer. The Tween 40 control system exhibited moderate stabilization, with a DI of approximately 20% after 24 h. This is consistent with the steric stabilization behavior of non-ionic surfactants (Cai et al., 2022), though insufficient for prolonged stability. In contrast, all MXene-Tween 40 hybrid emulsions showed significantly enhanced stability, consistently outperforming the control. At 0.1 and 0.5 wt% MXene (MXene-0.1 and MXene-0.5), no phase separation was observed after 24 h (DI = 0%), while only minimal demulsification occurred at higher concentrations (DI = 0.6% and 1.0% for MXene-1.0 and MXene-1.5, respectively). This enhanced performance reflects the cooperative interaction between MXene and Tween 40 at the oil–water interface, as neither component alone achieved comparable stability.

A similar synergistic effect was observed by Pei et al. (2018), who varied cetyltrimethylammonium bromide (CTAB) concentrations (0.01–0.5 wt%) in emulsions stabilized with 0.4 wt% SiO_2 nanoparticles. They reported that 0.5 wt% CTAB produced the most stable emulsions over 60 days, with stability improving beyond the 0.1 wt% threshold but decreasing below it. In our system, Tween 40 rapidly adsorbs to the interface, reducing the interfacial tension and forming a hydrated polyoxyethylene layer that provides steric stabilization (Cai et al., 2022; Murasiewicz and Illienko, 2024). This steric barrier facilitates even distribution and interfacial anchoring of MXene nanosheets. Once adsorbed, the high aspect ratio and sheet-like morphology of MXene contribute to the formation of a contiguous mechanical barrier that reinforces droplet integrity. Moreover, hydrogen bonding between the –OH groups on the MXene surface and the ethylene oxide chains of Tween 40, along with van der Waals interactions between the surfactant's alkyl tails and the oil phase, further enhance interfacial cohesion (Fereidooni Moghadam et al., 2015; Wang et al., 2024; Xu et al., 2022; Yekeen et al., 2020). Comparable synergistic mechanisms have been observed in other hybrid Pickering systems, including ZnO nanoparticles with Gemini surfactants (Fereidooni Moghadam et al., 2015), and SiO_2 nanoparticles with sodium dodecyl sulfate (SDS) or cetyltrimethylammonium bromide (CTAB) (Maurya and Mandal, 2018), where enhanced interfacial films and reduced interfacial tension result in more stable emulsions (Fereidooni Moghadam et al., 2015; Maurya and Mandal, 2018). Sharma et al. (2015) also demonstrated improved thermal stability in emulsions formulated with polyacrylamide, SDS, and various nanoparticles (e.g., SiO_2, clay, CuO). Our findings align with these studies and further underscore the practical relevance of the MXene-Tween 40 approach for EOR and related oilfield applications. In cEOR, stable fine emulsions are critical for efficient propagation through reservoir pore networks, resistance to coalescence under salinity and temperature stress, and consistent oil mobilization (Kaushik et al., 2024). The observed stability of MXene-Tween 40 hybrid emulsions directly supports these operational requirements.

A concentration-dependent effect was clearly observed during long-term stability testing over 30 d, as shown in Fig. 4. At 0.1 wt% MXene, the emulsion remained highly stable, with DI values of 0 at day 1, and gradual increases to 4.0%, 8.0%, and 13.0% at 10, 20, and 30 d, respectively. This behavior reflects effective interfacial adsorption and coverage by MXene nanosheets, aided by the stabilizing action of Tween 40. At 0.5 wt%, a moderate increase in DI was observed, with values rising from 0 at day 1 to 5.4%, 11.4%, and 17.0% at 10, 20, and 30 d, respectively. The higher DI suggests emerging nanoparticle aggregation in the continuous phase (Ming et al., 2023), which reduces the effective surface-active fraction. Increasing the MXene concentration to 1.0 wt% accelerated this trend, with DI values rising from 0.6% at day 1 to 8.0%, 11.8%, and 20.0% at 10, 20, and 30 d, respectively, indicating that excessive nanoparticles promote aggregation and reduce stability. At 1.5 wt% MXene, this effect became even more pronounced, with DI values of 1% at day 1 and jumps to 10.0%, 15.8%, and 25.0% at 10, 20, and 30 d, respectively. This pronounced phase separation at higher DL-$Ti_3C_2T_x$ MXene concentrations is attributed to excessive nanoparticle aggregation, which disrupts interfacial coverage and may facilitate bridging flocculation, where aggregates physically link multiple droplets and thereby promote coalescence (Yang et al., 2017; Zhao et al., 2022). These results confirm the presence of an optimal MXene concentration near 0.1 wt%. Beyond this threshold, interfacial saturation occurs and excess MXene remains in the bulk phase, where it tends to aggregate due to weakened electrostatic and steric repulsion, consistent with DLVO theory (Hatchell et al., 2022). These aggregates not only fail to adsorb at the interface but may also contribute to destabilization by promoting bridging interactions (Kondaraju et al., 2012). Similar behavior has been reported in emulsions stabilized by PEG-coated SiO_2 and other solid particles (Hatchell et al., 2022; Yang et al., 2024). Wang et al. (2024) reported a similar concentration-dependent stability trend in O/W emulsions stabilized by amphiphilic SiO_2 nanoparticles and a non-ionic surfactant (OP-50). Stability improved with increasing nanoparticle concentration up to an optimal value of 0.1 wt%, but declined at higher concentrations due to aggregation and reduced interfacial efficiency. These findings emphasize the need to optimize both nanoparticle and surfactant concentrations in hybrid systems to maximize stability.

As illustrated in Fig. 5, the stability behavior of DL-$Ti_3C_2T_x$ Pickering emulsions varies markedly with MXene concentration. At low concentrations (e.g., 0.1 wt%), MXene nanosheets effectively adsorb at the oil–water interface, forming a continuous protective shell around the droplets that enhances stability (Sun et al., 2022a). However, as the concentration increases (e.g., $\geq$ 0.5 wt%), excess nanosheets remain suspended in the bulk aqueous phase. These unadsorbed particles tend to crowd the system, leading to aggregation and the onset of interfacial bridging between droplets. This bridging effect compromises interfacial integrity and promotes coalescence, thereby diminishing the overall stabilizing efficiency of MXene (Lu et al., 2024). The schematic in Fig. 5 emphasizes the importance of optimizing MXene loading to maintain effective interfacial coverage while avoiding destabilizing bulk-phase interactions. Similar observations were made by Zhao et al. (2020), who reported the formation of Janus MXene nanosheets by electrostatically attaching positively charged polystyrene to negatively charged MXene surfaces. These

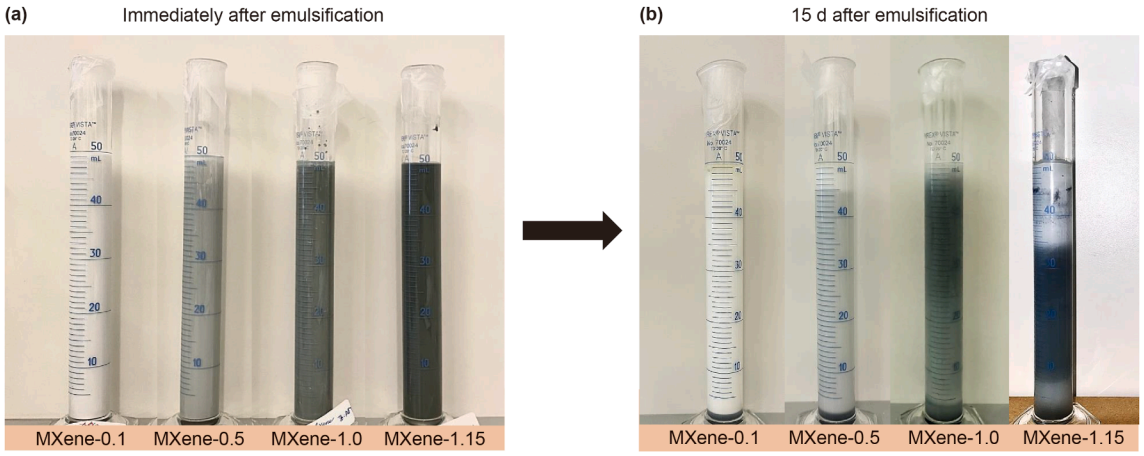

Fig. 4. Visual representation of phase separation in DL-$Ti_3C_2T_x$ MXene-stabilized emulsions at different concentrations (0.1, 0.5, 1.0, and 1.5 wt%). (**a**) Immediately after emulsification. (**b**) After 15 d.

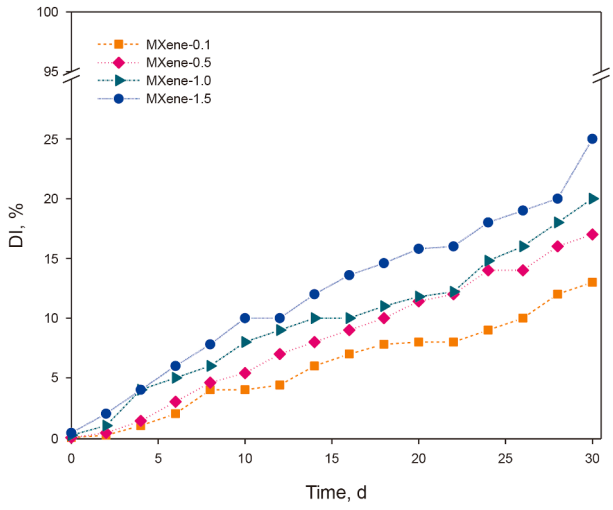

Fig. 5. Demulsification of DL-$Ti_3C_2T_x$ MXene-stabilized Pickering emulsions at varying concentrations.

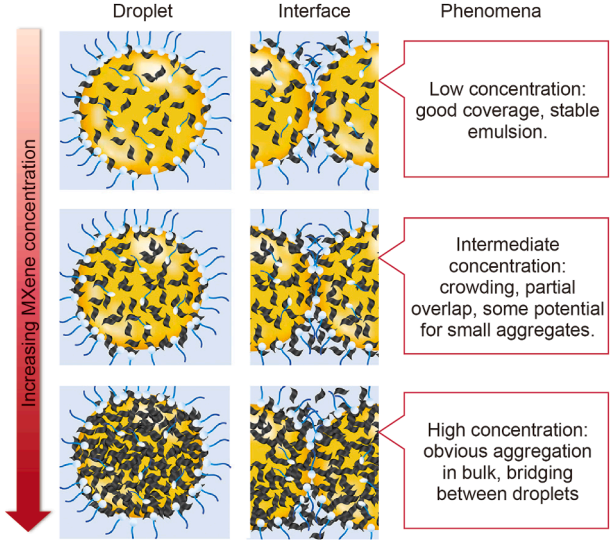

Fig. 6. Schematic representation of concentration-dependent interfacial behavior in DL-$Ti_3C_2T_x$-stabilized Pickering emulsions. The figure illustrates how increasing MXene concentration shifts the system from uniform interfacial coverage to aggregation and bridging flocculation.

Janus particles successfully stabilized toluene-in-water emulsions, illustrating the importance of dual-phase interaction in enhancing interfacial behavior.

Collectively, these findings demonstrate that the synergistic combination of MXene and Tween 40 yields Pickering emulsions with significantly enhanced stability. This enhancement arises from the complementary roles of each component at the oil–water interface. The MXene-Tween 40 system offers a rational platform for designing robust, surfactant-lean emulsions suitable for EOR and other oilfield applications. Microscopic observations (see Fig. 6) further support this trend. At lower MXene concentrations such as 0.1 wt%, the emulsions consisted of small, uniformly dispersed droplets with minimal aggregation in the continuous phase. In contrast, emulsions containing higher MXene concentrations exhibited dark circular features under the microscope, corresponding to large particle aggregates. These observations provide visual evidence of bulk-phase clustering and interfacial destabilization.

3.3. Microscopic structural analysis

The droplet morphology and microstructure of DL-$Ti_3C_2T_x$ MXene-stabilized Pickering emulsions were examined using optical microscopy, as shown in Fig. 7. Distinct changes in droplet size and uniformity were observed with varying MXene concentrations, providing mechanistic insight into the relationship between nanoparticle loading and emulsion stability. At the lowest MXene concentration (MXene-0.1), the emulsions displayed small, well-dispersed droplets, indicating uniform adsorption of nanosheets at the oil–water interface. This even interfacial coverage effectively suppressed droplet coalescence, resulting in a stable emulsion with a narrow size distribution (Behera et al., 2024).

Importantly, such fine and stable emulsions are highly advantageous for EOR applications. Smaller droplets are more likely to travel through the intricate pore networks of reservoir rocks without causing plugging or rapid coalescence, thereby enabling deeper penetration and more efficient oil displacement during flooding operations (Maurya and Mandal, 2018). Upon increasing the MXene concentration to 0.5 wt% (MXene-0.5), a modest increase in droplet size was observed, along with the emergence of subtle aggregation. These changes are attributed to intensified particle–particle interactions within the continuous phase, which

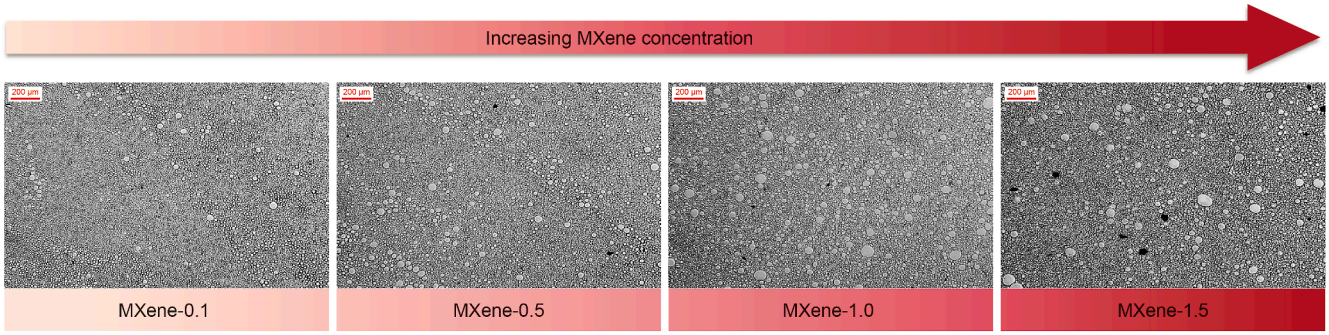

Fig. 7. Microstructure of DL-$Ti_3C_2T_x$ MXene-stabilized Pickering emulsions at varying concentrations.

reduce the availability of nanosheets for interfacial stabilization (Feng et al., 2020). Boostani et al. (2020) reported a similar trend for hordein nanoparticles, where Pickering emulsions at lower concentrations yielded smaller and more stable droplets, while higher loadings promoted aggregation and larger droplet formation, ultimately decreasing overall emulsion stability. At the highest tested concentration (MXene-1.5), the Pickering emulsions exhibited significant microstructural changes. Large, irregularly shaped droplets appeared, accompanied by visible flocculation and clustering of MXene nanosheets. The presence of such aggregates indicates that the system has surpassed a critical nanoparticle loading threshold, where particle–particle interactions overwhelm the stabilizing benefits of interface adsorption (Kondaraju et al., 2012). These findings are consistent with previous reports, including those by Boostani et al. (2020) and Feng et al. (2020), who demonstrated that excessive nanoparticle concentrations can reduce emulsion stability by promoting flocculation and inefficient interfacial coverage. This loss of uniform particle dispersion can potentially limit the efficiency of emulsion transport through tight reservoir pores, reinforcing the importance of optimizing nanoparticle dosage for field applications. Nevertheless, the absence of complete phase separation even after 30 days at high MXene concentrations underscores the inherent stabilizing capacity of MXene nanosheets. These observations underscore the importance of optimizing MXene concentration to achieve a balance between effective interfacial coverage and prevention of aggregation.

3.4. Zeta potential analysis

Zeta potential measurements were conducted to assess the electrostatic stabilization of MXene-stabilized Pickering emulsions, as shown in Fig. 8. These measurements indicate the surface charge of emulsion droplets and the repulsive forces between them, which are crucial for preventing coalescence and maintaining emulsion stability. Emulsions with zeta potential magnitudes exceeding ±30 mV are generally considered electrostatically stable due to sufficient repulsive interactions (Abu Zaid et al., 2025). For the control system (MXene-0.0), which was stabilized solely by 0.5 wt% Tween 40 and 0.15 wt% AMEREL® 1500, a zeta potential of −45 mV was observed (Fig. 8), indicating strong electrostatic stabilization. Although Tween 40 is a non-ionic surfactant, its polyoxyethylene head groups can adsorb hydroxide ions (OH^-) at the oil–water interface, imparting a net negative surface potential. Similar behavior has been reported for other polyoxyethylene-based surfactants such as Tween 60 and Tween 80, where hydrogen bonding and oxonium formation contribute to negative zeta values (Hong et al., 2018). MXene nanosheets are inherently hydrophilic due to surface terminations like –OH and =O and typically exhibit zeta potentials between −30 and −40 mV at neutral pH (Yadav et al., 2024). The point of zero charge (PZC) for MXene dispersions was found at a pH of approximately 2.45 (Fig. 8(a)). Below this pH, MXene surfaces carry a net positive charge, while above it, they are negatively charged. Since the emulsions in this study had a pH between 6 and 9, the MXene surfaces were strongly negatively charged, contributing to electrostatic stabilization. The zeta potential data for DL-$Ti_3C_2T_x$ MXene-stabilized Pickering emulsions with 0.5 wt% Tween 40 are presented in Fig. 8(b).

As the MXene concentration increased, the magnitude of the zeta potential decreased slightly. Specifically, the zeta potentials for MXene-0.1, MXene-0.5, MXene-1.0, and MXene-1.5 were −49.76, −47.70, −43.71, and −37.06 mV, respectively. While higher concentrations of stabilizing particles or surfactants would ideally enhance surface charge density and improve stability (Ming et al., 2023), the measured values revealed a reverse trend, suggesting that increased MXene loading led to partial aggregation and reduced interfacial dispersion efficiency. Thieme et al. (1999) reported that strong interfacial particle–particle interactions can induce aggregation, reducing the effective surface area available for interfacial stabilization. Microscopic images support this interpretation (see Fig. 7), showing the presence of large black aggregates at higher nanocomposite loadings. These aggregates impair particle dispersion and limit their ability to stabilize the oil–water interface, ultimately diminishing emulsion stability. These results highlight the importance of balancing MXene concentration to maintain optimal emulsion behavior. While low concentrations enhance electrostatic repulsion and particle dispersion, higher concentrations induce aggregation and reduce interfacial effectiveness. A similar observation has been reported in blended emulsifier systems. For instance, Yang et al. (2025b) studied emulsified asphalts stabilized with cationic and non-ionic surfactants and found that, although increasing emulsifier dosage initially improved zeta potential and stability, further increases caused double-layer compression, micelle formation, and eventual destabilization. Their findings confirm that the key to sustained emulsion stability is a favorable interfacial structure rather than the absolute charge magnitude.

3.5. Droplet size distribution

The stability of Pickering emulsions is closely linked to the size distribution of dispersed droplets, as smaller and more uniform droplets generally resist coalescence and facilitate effective transport in porous media (Adil and Onaizi, 2022). Fig. 9 summarizes the effect of $Ti_3C_2T_x$ MXene concentration on the average droplet size at a fixed Tween 40 content (0.5 wt%). The control emulsion (MXene-0.0) containing only surfactant and antifoam

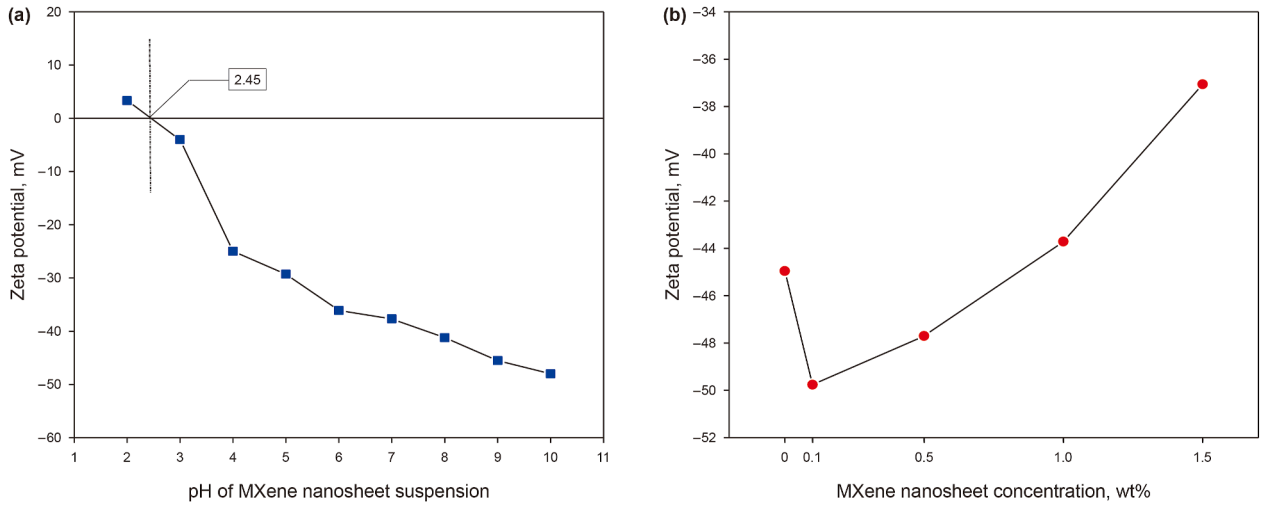

Fig. 8. Zeta potential analysis of DL-$Ti_3C_2T_x$ in different media. (**a**) Effect of pH on the zeta potential of DL-$Ti_3C_2T_x$ suspensions. (**b**) Effect of DL-$Ti_3C_2T_x$ concentration on the zeta potential of Pickering emulsions.

produced small droplets (~0.13 μm), highlighting the initial stabilizing action of Tween 40 via interfacial tension reduction and formation of a protective steric layer (Song et al., 2024). However, this system showed only moderate stability, as significant phase separation was observed within 24 h (see Section 3.2). The introduction of $Ti_3C_2T_x$ MXene led to a concentration-dependent increase in the mean droplet size: 3.43 μm (MXene-0.1), 5.02 μm (MXene-0.5), 7.16 μm (MXene-1.0), and 16.39 μm (MXene-1.5). Unlike traditional Pickering systems, where increasing nanoparticle concentration typically leads to smaller droplet sizes due to improved interfacial coverage (Pang et al., 2024), the present results showed an opposing trend. This behavior is attributed to the aggregation of MXene nanosheets at elevated loadings, which limits their availability for interfacial adsorption. Microscopy confirmed that increased MXene concentrations promoted stronger particle–particle interactions within the continuous phase (see Fig. 7), leading to bulk aggregation, depleted interfacial coverage, and ultimately the formation of larger droplets. Such aggregation also fosters flocculation and bridging between droplets, further undermining emulsion stability (Kondaraju et al., 2012). These findings align with previous studies reporting threshold-dependent destabilization in nanoparticle-stabilized systems. For example, Liu et al. (2023) demonstrated that walnut protein nanoparticles above a critical concentration (i.e., 2 wt%) induced interfacial saturation and aggregation. Similarly, Zhou et al. (2020) observed that zein-tannic acid Pickering emulsions exhibited optimal droplet size and stability only at moderate nanoparticle concentrations, while higher dosages promoted bridging flocculation and droplet clustering. A comparable effect was reported by Yang et al. (2025b) for asphalt-surfactant blends, where excessive emulsifier concentration led to particle growth and instability due to double-layer compression and aggregation. These studies highlight the necessity of optimizing the nanoparticle-to-surfactant ratio to achieve effective interfacial coverage and maintain minimal droplet size. From an EOR perspective, the ability to produce fine, stable emulsions is crucial for maximizing sweep efficiency and improving oil displacement in porous reservoir media. Emulsions with small, well-dispersed droplets are less prone to coalescence and more capable of navigating complex pore structures, facilitating deeper penetration and improved oil mobilization (Zhang et al., 2010).

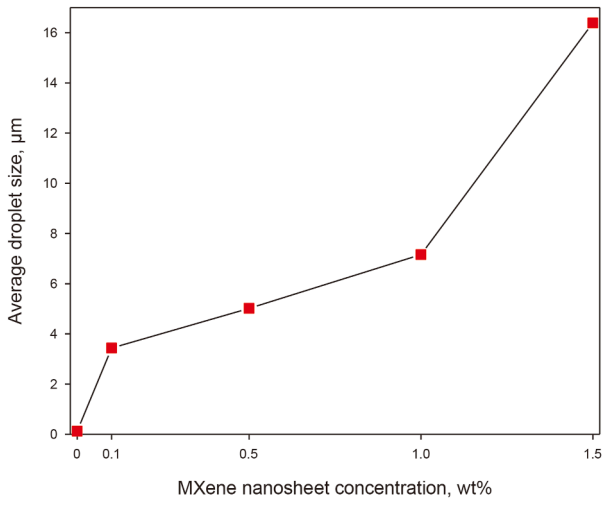

Fig. 9. Average droplet sizes of Pickering emulsions at varying DL-$Ti_3C_2T_x$ MXene concentrations.

The MXene-Tween 40 system, particularly at 0.1 wt% MXene, offered an effective balance: droplet sizes remained below the threshold for pore blocking, while emulsion stability was preserved over extended durations. Additionally, Rezaei et al. (2020) reported that alpha-olefin sulfonate (AOS) surfactant combined with hydrophilic SiO_2 NPs significantly improved oil recovery in carbonate reservoirs. However, despite these advancements, challenges remain. For instance, aggregation of nanoparticles under reservoir conditions can still occur due to changes in salinity, pH, or temperature, potentially leading to pore blockage and reduced permeability. Previous studies have proposed various strategies to mitigate this issue. For example, Zhao et al. (2024a) used lauramidopropyl hydroxy sulfobetaine in combination with SiO_2 to form a stable nanofluid that improved oil recovery during spontaneous imbibition. Similarly, Kumar et al. (2022) reported that a nanofluid composed of positively charged Ludox SiO_2 NPs and Aerosol-OT (AOT) surfactant effectively reduced interfacial tension and altered core wettability, resulting in enhanced recovery.

3.6. IFT characteristics

The dynamic IFT behavior of MXene-stabilized Pickering emulsions was systematically evaluated to understand the relationship between nanoparticle concentration, interfacial properties, and emulsion stability. Fig. 10(a) presents the time-dependent IFT measurements for various MXene concentrations. In the absence of any emulsifier, the baseline IFT between diesel and deionized water is approximately 25 mN/m (Narayan et al., 2018), underscoring the need for effective interfacial modification in EOR formulations. Upon the addition of Tween 40 (0.5 wt%, MXene-0.0), the IFT sharply decreases to 7.33 mN/m at the initial measurement, confirming the surfactant's rapid adsorption and effectiveness in lowering interfacial energy. This progressive decline in interfacial tension not only facilitates emulsification but also contributes to wettability alteration and capillary pressure reduction, both of which are critical mechanisms for enhancing oil mobilization during chemical EOR processes (Pei et al., 2024; Zhao et al., 2024b). Over 1 h, the IFT further decreases to 4.08 mN/m, indicating continued adsorption of Tween 40 molecules at the oil–water interface until equilibrium was reached. Similarly, Qazi et al. (2020) demonstrated that CTAB, a cationic surfactant, reduces IFT and improves the mobility ratio in cEOR applications.

The introduction of $Ti_3C_2T_x$ MXene into the system produced an additional and progressive reduction in IFT. Initial values decreased sequentially to 5.49, 4.20, 2.85, and 1.71 mN/m as the MXene content increased from 0.1 to 1.5 wt%. After 1 h, the final IFT values for the same series reached 3.01, 2.42, 1.58, and 0.86 mN/m, respectively. This significant trend is attributed to the high interfacial activity of MXene nanosheets, which stems from their sheet-like morphology and the presence of dense surface functional groups such as –OH, –F, and =O. These groups promote strong adsorption at the oil–water interface and support the formation of a dense, continuous interfacial film (Natalya et al., 2022).

As shown schematically in Fig. 10(b), MXene nanosheets, in cooperation with Tween 40 molecules, anchor at the interface, replacing direct oil–water contact with a thermodynamically stable composite layer. This behavior is widely observed in nanoparticle-stabilized emulsions and contributes to effective IFT reduction (Sun et al., 2022b). Compared to spherical, rod-like, or wire-shaped nanoparticles, MXene nanosheets demonstrate higher interfacial activity (Liang et al., 2022; Qu et al., 2020, 2021) and are thus more effective in modifying interfacial behavior. It is important to note, however, that lower IFT alone does not ensure enhanced emulsion stability across all concentrations. Despite the continued IFT reductions at higher MXene concentrations, improved stability was not consistently achieved. At loadings above 0.5 wt%, significant aggregation of nanosheets in the continuous phase was observed, as reflected in both demulsification index data and microscopic imaging (see Sections 3.2 and 3.5). Aggregation disrupts interfacial coverage and facilitates bridging flocculation, where clusters of MXene particles connect multiple droplets. This promotes phase separation even when IFT is low. Such decoupling between IFT and stability has been previously reported in nanoparticle-stabilized emulsions, where particle overloading can weaken the stabilizing film and promote droplet coalescence (Ghaffarkhah et al., 2024). The combined effect of Tween 40 and MXene is essential for rapid IFT reduction and initial emulsion stabilization. Hydrogen bonding between the hydroxyl groups of Tween 40 and those on the MXene surface, along with van der Waals interactions between the surfactant tails and diesel, contributes to the development of a compact interfacial film (Fereidooni Moghadam et al., 2015; Wang et al., 2024; Xu et al., 2022; Yekeen et al., 2020), as depicted in Fig. 10(b). This composite interfacial layer plays a critical role in sustaining emulsion stability at optimized concentrations. However, as the MXene content increases beyond the interfacial saturation threshold, steric and electrostatic repulsions hinder further adsorption. Excess MXene then accumulates in the aqueous phase, promoting particle–particle aggregation and bridging flocculation, which ultimately reduces the effectiveness of interfacial stabilization (Feng et al., 2020).

These observations reinforce that while lowering IFT is important for emulsion formation, it is not the sole determinant of

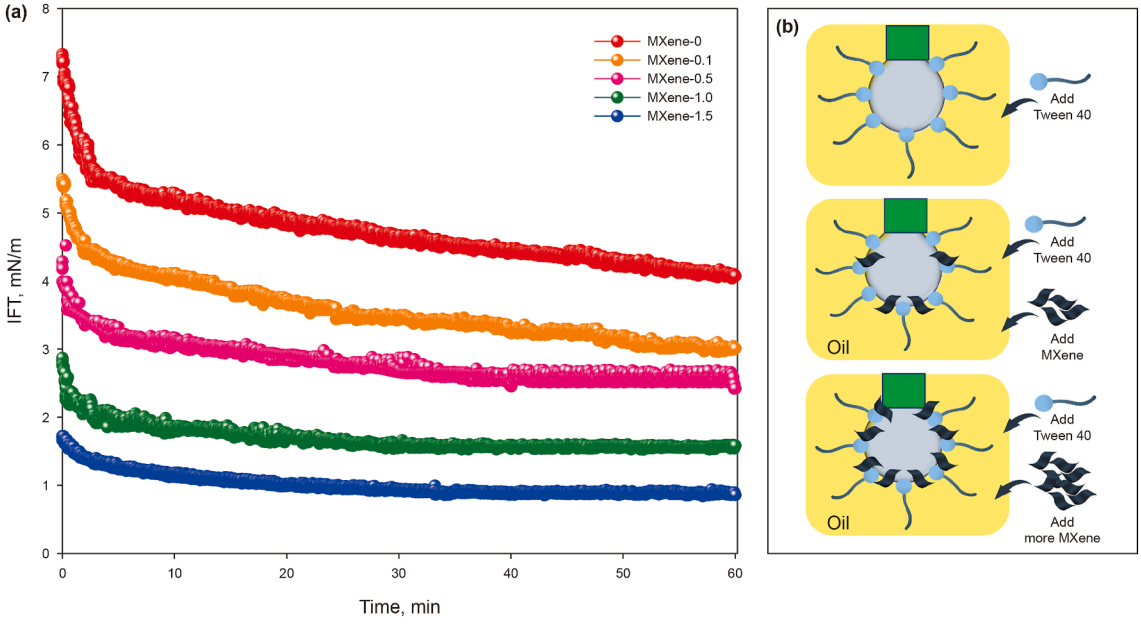

Fig. 10. (**a**) Time-dependent IFT reduction for Pickering emulsions stabilized with different concentrations of MXene, illustrating enhanced interfacial activity at higher loadings. (**b**) Schematic representation of the adsorption of DL-$Ti_3C_2T_x$ MXene nanosheets and Tween 40 molecules at the oil–water interface, highlighting their cooperative roles in forming a stable interfacial film.

stability, particularly in systems with high nanoparticle concentrations. As more $Ti_3C_2T_x$ MXene is introduced, the interface becomes saturated, and excess particles may aggregate or form bridges between droplets, which undermines long-term emulsion integrity (Wang et al., 2020). This behavior aligns with DLVO theory and prior studies of Pickering emulsions, where optimal nanoparticle–surfactant ratios are critical for balancing IFT reduction and maintaining effective stabilization (Blijdenstein et al., 2004; Kalashnikova et al., 2012). Although Tween 40 facilitates IFT reduction and aids in MXene dispersion at the interface, it cannot fully prevent nanoparticle aggregation at elevated concentrations. Similar trends have been reported in other nanoparticle–surfactant systems. For instance, in ZnO/CTAB-stabilized emulsions, further IFT reduction at high nanoparticle concentrations did not enhance stability due to increased particle bridging and aggregation, which caused larger droplets and accelerated phase separation (Fereidooni Moghadam and Azizian, 2014). Jiang et al. (2021) reported that the concentration of hydrophobic SiO_2 NPs significantly influenced the crude oil–water IFT in the presence of the non-ionic surfactant Span 80. The IFT reduction achieved in the nanoparticle–surfactant system exceeded that obtained with the surfactant alone, highlighting the critical role of nanoparticles in modifying interfacial properties. Tliba et al. (2025) showed that functionalizing SiO_2 NPs with anionic surfactants (i.e., ALS and SOS) led to a substantial reduction in oil–water IFT compared to either the surfactants or nanoparticles alone. At equivalent doses (100 ppm), the IFT for ALS and SOS alone remained above 10 mN/m, whereas ALS-NP and SOS-NP systems reduced IFT to below 2 mN/m, reaching values as low as 10^{-2} to 10^{-4} mN/m when 0.1 wt% alkali was added. This sharp drop was attributed to improved surfactant adsorption via NP grafting, which formed a more stable and densely packed interfacial film. However, they also observed that increasing nanoparticle concentrations beyond 100 ppm led to greater particle aggregation and a rise in creaming index, emphasizing that while IFT decreased, emulsion stability did not always improve proportionally mirroring the trends observed in MXene-based systems.

3.7. Rheological characterization of Pickering emulsions

The application of Pickering emulsions in EOR requires a thorough understanding of their rheological behavior, as it directly affects flow performance, mobility control, and structural integrity during injection and transport through porous reservoirs. Adjusting viscosity and flow characteristics is essential for displacing residual oil effectively, minimizing permeability in high-water-cut zones, and preserving emulsion stability under varying shear and thermal conditions. Moreover, several studies have demonstrated that emulsions with enhanced bulk viscosity and viscoelasticity, achieved through nanoparticle–surfactant synergy, can significantly improve sweep efficiency and oil recovery in porous media, even under high temperature and salinity (Pei et al., 2024; Rattanaudom et al., 2023). In this context, the rheological characteristics of DL-$Ti_3C_2T_x$ MXene-stabilized Pickering emulsions under different shear rates, temperatures, and NP concentrations have been investigated to assess their suitability for EOR applications. The analysis encompasses the transition from Newtonian to non-Newtonian behavior, shear-thinning effects, and the impact of temperature on viscosity profiles. Additionally, different rheological models have been employed to quantify this behavior, providing a foundation for optimizing MXene-based emulsions for field-relevant flow scenarios.

3.7.1. Viscosity responses to shear rate at different MXene concentrations

The rheological behavior of DL-$Ti_3C_2T_x$ MXene-stabilized Pickering emulsions was evaluated by measuring viscosity over a range of shear rates (1–600 s^{-1}) and temperatures (25, 45, and 65 °C). The results, shown in Fig. 11, revealed distinct flow patterns depending on MXene concentration and applied shear rate. At the lowest MXene concentration of 0.1 wt% (MXene-0.1 emulsion, Fig. 11(a)), the emulsions displayed Newtonian behavior, where viscosity remained constant across all shear rates. This indicates that the internal structure of the emulsion was stable, with minimal particle–particle interactions affecting the viscosity (Liu et al., 2023). Such stable viscosity at low MXene content is desirable in EOR applications, as high viscosity at low shear rates enhances mobility control and oil recovery (Sastry et al., 1999). As the MXene concentration increased to 0.5 wt% (Fig. 11(b)), 1.0 wt% (Fig. 11(c)), and 1.5 wt% (Fig. 11(d)), the Pickering emulsions began to exhibit shear-thinning behavior, where the viscosity decreased with increasing shear rate. This non-Newtonian pseudoplastic response arises from the re-alignment of dispersed droplets and DL-$Ti_3C_2T_x$ nanosheets in the direction of flow, which lowers internal resistance (Kour et al., 2024; Xu et al., 2021). This behavior is typical for emulsions with higher solid content, where particles align under shear and contribute to a viscosity drop. Additionally, viscosity increased with MXene concentration at a given shear rate, due to enhanced network formation within the continuous phase. At higher loadings, DL-$Ti_3C_2T_x$ nanosheets form denser internal structures, increasing resistance to flow, particularly at low shear. This transition from Newtonian to non-Newtonian flow highlights the growing importance of particle–particle and particle–surfactant interactions in shaping emulsion rheology. These networks dynamically respond to shear by breaking down under stress and reforming when the stress is released (Szumała and Luty, 2016; Yan et al., 2010). However, a notable limitation at elevated MXene concentrations is the tendency of nanosheets to aggregate or restack, driven by van der Waals attractions and limited electrostatic repulsion. This aggregation leads to non-uniform particle distribution and increases bulk viscosity without proportionally enhancing interfacial stabilization, as some particles remain in the continuous phase rather than adsorbing at the interface. While this contributes to viscosity buildup, it may compromise interfacial efficiency and emulsion uniformity (Ahmed et al., 2024; Rezvani et al., 2024). Comparable effects were observed by Qiu and Mamora (2010), who found that the bulk viscosity of a SiO_2-stabilized emulsified xylene system increased sharply when nanoparticle content exceeded 2 wt%, highlighting how excessive NP content can disproportionately thicken the continuous phase.

Temperature also influenced viscosity across all samples. As temperature increased from 25 to 65 °C, viscosity decreased at a given shear rate. This temperature-thinning response is attributed to reduced intermolecular forces and increased molecular motion at higher temperatures, both of which promote flow (Shah et al., 2020). This behavior is favorable for EOR applications, where emulsions must remain sufficiently flowable under reservoir thermal conditions (Kumar et al., 2017; Xie et al., 2018). Furthermore, emulsions generally possess higher viscosity than water, which helps suppress viscous fingering and enhances sweep efficiency during injection, particularly in high-permeability or heterogeneous zones (Rezvani et al., 2024). The increased viscosity of nanoparticle-based emulsions with surfactants can reduce their mobility, enabling more uniform displacement of trapped oil and minimizing bypassing, both of which are essential for improved oil

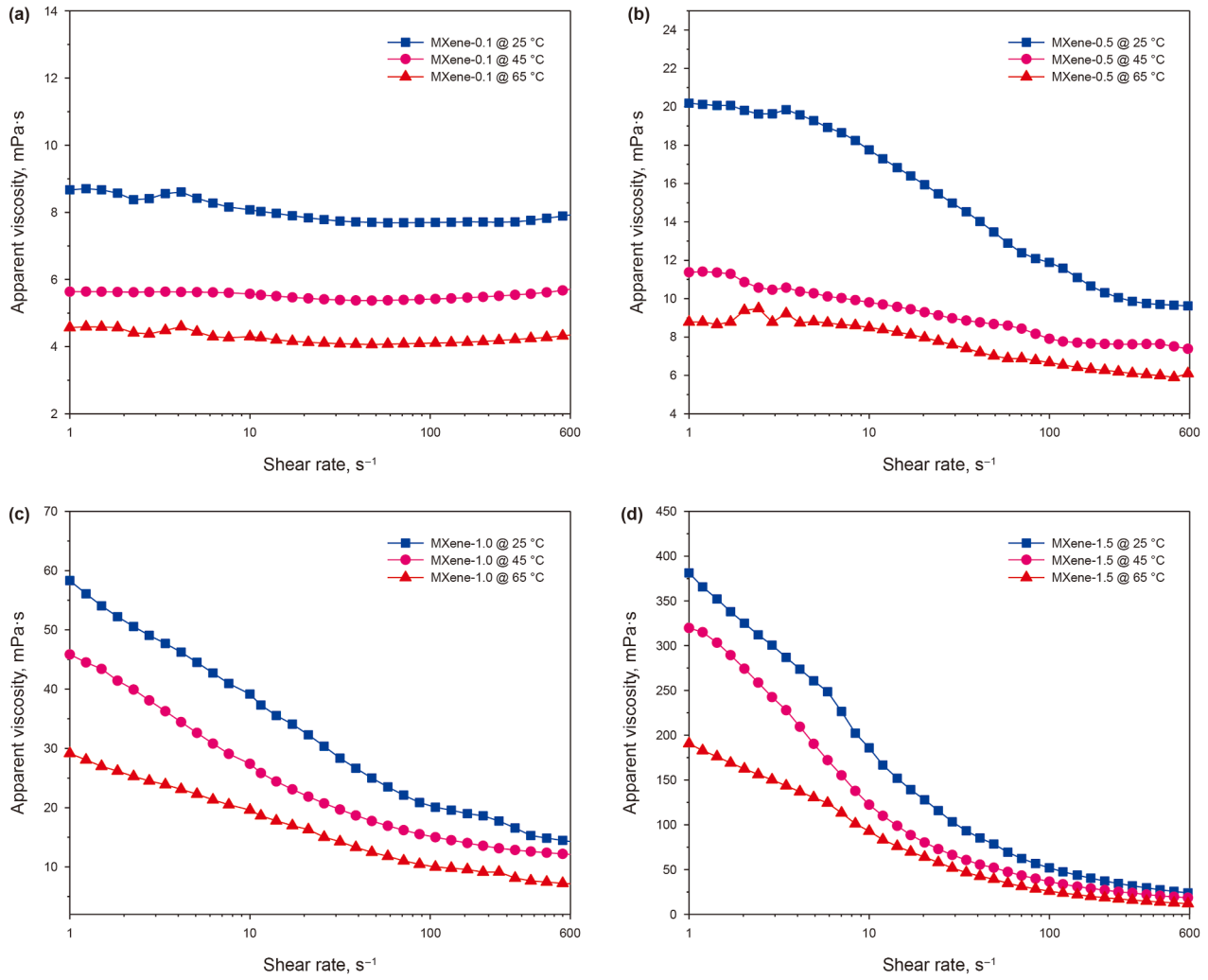

Fig. 11. Apparent viscosity versus shear rate for DL-$Ti_3C_2T_x$ MXene-stabilized Pickering emulsions at different concentrations and temperatures. The panels represent emulsions stabilized with varying MXene concentrations: (**a**) MXene-0.1, (**b**) MXene-0.5, (**c**) MXene-1.0, and (**d**) MXene-1.5.

recovery under reservoir-relevant conditions (Abu Zaid et al., 2025). Similar temperature-dependent rheological responses have been reported for other Pickering systems (Cui et al., 2024; Kour et al., 2024; Kumar et al., 2017; Li et al., 2021; Liu et al., 2023, 2024; Xu et al., 2021; Zhang and Yu, 2023).

3.7.2. *Influence of frequency on viscoelastic moduli of MXene-stabilized Pickering emulsions*

The viscoelastic properties of DL-$Ti_3C_2T_x$ MXene-stabilized Pickering emulsions were investigated through dynamic oscillatory measurements, and the obtained results are shown in Fig. 12. Pickering emulsions with varying concentrations of DL-$Ti_3C_2T_x$ MXene nanosheets (from 0.1 up to 1.5 wt%) were tested at 25, 45, and 65 °C, covering a frequency range from 1 to 600 rad/s to simulate different operational conditions. The storage modulus (G') and loss modulus (G'') were measured to characterize the emulsion's elastic and viscous behavior.

At low angular frequencies, all DL-$Ti_3C_2T_x$ MXene-stabilized Pickering emulsions showed G' values higher than G'', indicating a solid-like viscoelastic behavior (Zhang et al., 2022). This suggests that the DL-$Ti_3C_2T_x$ MXene nanosheets effectively adsorb at the oil–water interface, creating emulsions with a rigid network structure. This network structure resists deformation under low frequencies due to strong particle–particle interactions (Feng et al., 2020). However, as the frequency increased, the emulsions transitioned from solid-like to liquid-like behavior. At a specific crossover frequency (SF), where G' and G'', intersect, the Pickering emulsions began to exhibit viscous dominance, indicating a shift to more liquid-like behavior (Kumar and Mandal, 2018a). This transition is caused by the breakdown of the rigid network formed by DL-$Ti_3C_2T_x$ MXene nanosheets as the deformation rate increases (Niraula et al., 2004). For example, at 25 °C, the crossover point for the emulsion with 0.1 wt% MXene is at 1.10 rad/s, while for the 1.5 wt% emulsion, the SF increased to 18.02 rad/s, demonstrating that higher MXene concentrations help maintain the elastic properties over a broader frequency range before transitioning to a viscous state.

Temperature had a notable impact on the viscoelastic properties of the DL-$Ti_3C_2T_x$ MXene-stabilized Pickering emulsions. As the temperature increased from 25 to 65 °C, the SF shifted to higher frequency values, indicating that the Pickering emulsions retained their elastic characteristics over a broader range of applied frequencies at elevated temperatures. For example, in the 0.5 wt% Pickering emulsion, the SF increased from ~2.35 rad/s at 25 °C to ~21.04 rad/s at 65 °C (Table 1). This trend suggests that the emulsions became more solid-like as the temperature increased,

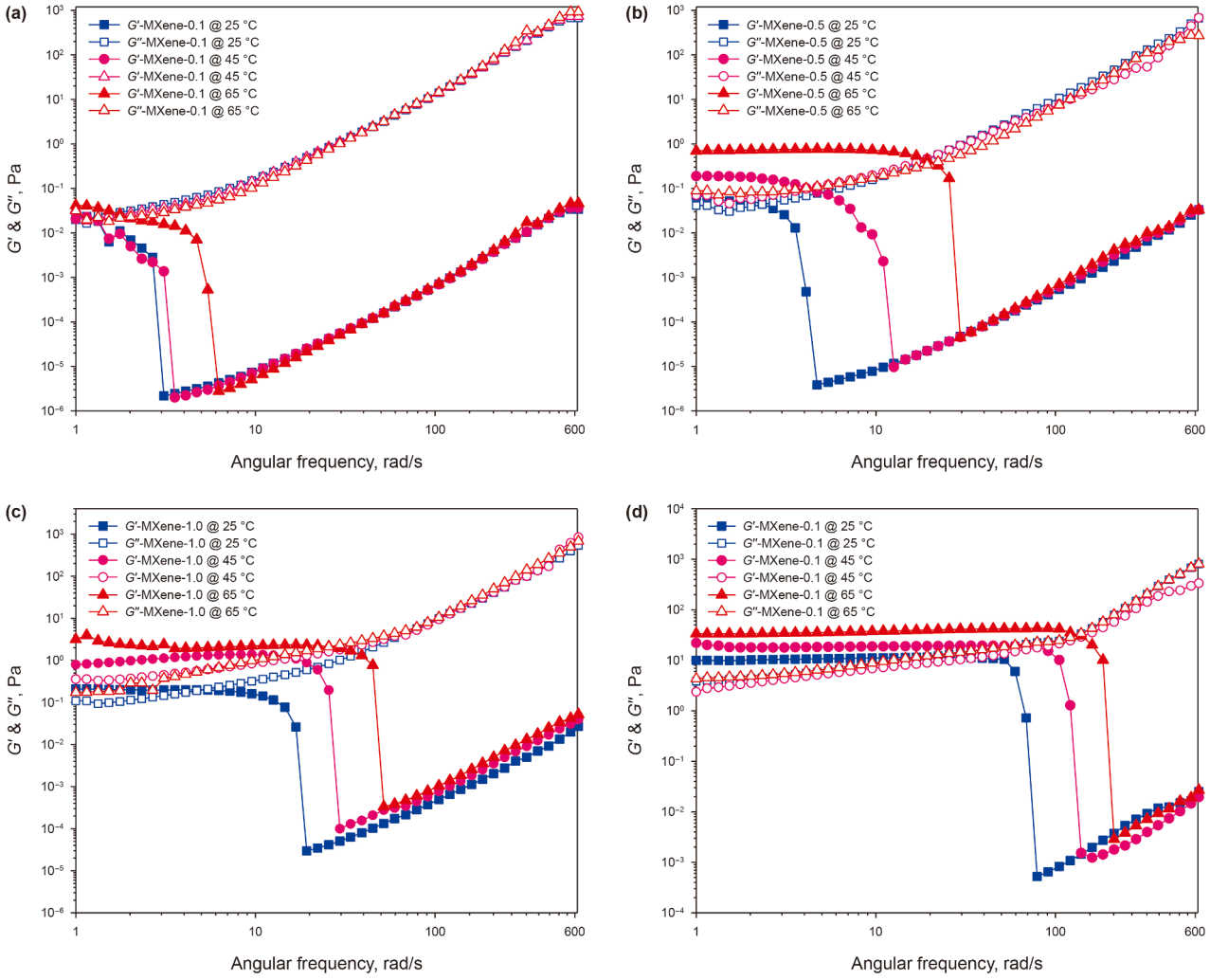

Fig. 12. Frequency-dependent G' and G'' for DL-$Ti_3C_2T_x$ MXene-stabilized Pickering emulsions at different concentrations and different temperatures. Panels represent emulsions with varying MXene concentrations: (**a**) MXene-0.1, (**b**) MXene-0.5, (**c**) MXene-1.0, and (**d**) MXene-1.5.

Table 1
SF at different temperatures for DL-$Ti_3C_2T_x$ MXene-stabilized emulsions.

Temperature, °C	SF, rad/s			
	MXene-0.1	MXene-0.5	MXene-1.0	MXene-1.5
25	~1.10	~2.35	~4.99	~18.02
45	~1.22	~4.18	~15.89	~81.34
65	~1.95	~21.04	~25.95	~132.30

Note: SF values were estimated using linear interpolation between data points where G' and G'' intersect.

likely due to intensified Brownian motion, which strengthens particle–particle interactions and enhances network formation within the emulsion (Jing and Song, 2017). As a result, the elastic nature of the Pickering emulsions becomes more pronounced, providing better stability under elevated thermal conditions. This property is particularly beneficial for EOR, where emulsions are expected to remain stable and resist structural breakdown under varying reservoir temperatures.

The concentration of DL-$Ti_3C_2T_x$ MXene nanosheets also played a critical role in modulating the viscoelastic behavior of the formulated emulsions. As the concentration increased from 0.1 to 1.5 wt%, both G' and G'' values increased, and the SF shifted to higher frequencies. For example, at 65 °C, the SF for the 0.1 wt% emulsion was ~1.95 rad/s, while for the 1.5 wt% emulsion, it reached ~132.30 rad/s under the same conditions (Table 1). This substantial increase indicates that higher concentrations of MXene enhance the resistance to deformation, allowing the emulsions to maintain elasticity over a wider range of applied stresses and temperatures. At higher concentrations, the DL-$Ti_3C_2T_x$ MXene nanosheets form a denser network, increasing the Pickering emulsion structural integrity. The ability to sustain elastic properties over a wide range of frequencies and temperatures suggests that DL-$Ti_3C_2T_x$ MXene-stabilized Pickering emulsions can effectively handle the complex flow dynamics encountered in EOR operations, thereby enhancing oil recovery and ensuring Pickering emulsion stability under challenging conditions.

Interestingly, beyond the crossover frequency, the G' modulus dropped sharply before increasing again, suggesting a complex restructuring within the Pickering emulsion. This non-monotonic behavior reflects short-time relaxation processes at higher frequencies, where the internal structure reorganizes under shear (Kumar and Mandal, 2018b). Additionally, the G' and G'' values remained relatively stable across the tested temperatures, indicating that the emulsions' structure at higher frequencies was less temperature-dependent. Similar observations have been reported

in other studies. For example, Feng et al. (2020) found that Pickering emulsions stabilized by gelatin NPs exhibited $G' > G''$ at low frequencies, transitioning to viscous behavior at higher frequencies. Likewise, Liu et al. (2023) reported that emulsions stabilized with nano-WalPI displayed solid-like behavior at 0.1–10 Hz but became more liquid-like at 10–100 Hz, depending on particle concentration. Another study by Xu et al. (2021) using emulsions stabilized by gliadin/sodium caseinate NPs also observed a shift in the crossover point with increasing particle concentrations, indicating greater stability and elasticity at higher particle content.

3.7.3. Temperature effect on viscosity of Pickering emulsion

Thermal stability is a critical factor in determining the performance of emulsions across various applications, making it essential to understand how viscosity changes with temperature variations (Pal, 1993). In this study, the effect of temperature on the viscosity of DL-$Ti_3C_2T_x$ MXene-stabilized Pickering emulsions was investigated during both heating (from 25 to 80 °C) and cooling (from 80 back to 25 °C) cycles, as shown in Fig. 13. For lower MXene concentrations (0.1 and 0.5 wt%), the Pickering emulsions exhibited a typical temperature-thinning behavior during heating, as illustrated in Fig. 13(a). The viscosity steadily decreased as the temperature increased, which is attributed to the increased kinetic energy of the emulsion droplets. Higher kinetic energy leads to enhanced Brownian motion, causing droplets to move more freely and reducing inter-droplet interactions, ultimately lowering the viscosity. In contrast, Fig. 13(b) shows the viscosity-temperature profiles for Pickering emulsions with higher MXene concentrations (1.0 and 1.5 wt%). During heating, these emulsions displayed a distinct non-linear behavior characterized by three regions. In Region I (from 25 to ~35–40 °C), the viscosity decreased due to thermal thinning, similar to what was observed at low concentrations. However, in Region II (from around 35–40 °C to 65–70 °C), a significant viscosity increase occurred, reaching a peak at a critical temperature (T_c). For example, the viscosity of the 1.0 wt% MXene Pickering emulsion increased from 12.75 mPa·s at 42 °C to 56.35 mPa·s at 67 °C, while the 1.5 wt% Pickering emulsion rose from 16.30 mPa·s at 37 °C to 83.63 mPa·s at 65.5 °C. This unusual increase suggests the formation of an internal network, driven by vigorous NP collisions and enhanced particle interactions at elevated temperatures. Similar trends have been reported in nanoparticle-stabilized systems. For instance, Sunny et al. (2011) observed a dramatic increase in viscosity at a critical temperature in dilute nanofluids containing sterically stabilized iron oxide and alumina NPs. They attributed this to the collapse of surfactant layers, which increased van der Waals attractions and led to the formation of interconnected structures. Below the critical temperature, particles remained under Brownian motion, resulting in lower viscosity due to the absence of such networks. This behavior aligns with the behavior observed in the high-concentration MXene Pickering emulsions. Lupu et al. (2023) observed a sol-to-gel transition in Pluronic F127 gels with the addition of ZnO NPs. The increases in gel strength and viscosity at elevated temperatures were influenced by both the concentration of NPs and their interaction with the gel matrix, similar to the gel-like behavior observed here in DL-$Ti_3C_2T_x$ MXene-stabilized emulsions. Such structural transitions are common in systems where NP interactions dominate the rheological response. Paola Marín Castaño et al. (2020) further emphasized temperature-induced structural changes in W/O crude emulsions. Their study found that elevated temperatures caused irreversible aggregation of droplets, resulting in higher apparent viscosity during cooling. This phenomenon is consistent with rheopexy (Fig. 14), where viscosity increases over time under constant shear due to structural buildup. In Region III (beyond the peak temperature), a decline in viscosity was observed, indicating network breakdown at higher thermal energies. This breakdown is likely due to intensified thermal motion, which disrupts aggregates and weakens stabilizing interactions. Desorption of surfactant layers or changes in the continuous phase viscosity may also contribute to the observed decrease.

During the cooling cycle, the viscosity profiles of the high-concentration emulsions deviated from their heating behavior, indicating hysteresis and irreversible structural changes. For example, in the 1.0 wt% MXene Pickering emulsion, the viscosity at 81 °C was approximately 34.89 mPa·s, significantly lower than its peak value of 56.35 mPa·s at 67 °C during heating. Similarly, for the 1.5 wt% MXene Pickering emulsion, the viscosity at 81 °C was 55.29 mPa·s, compared to its peak of 83.63 mPa·s at 65.5 °C during heating. This hysteresis suggests that irreversible aggregation occurred during heating, forming flocs that persisted during cooling. As a result, the emulsions did not fully return to their initial state, and viscosity at the end of the cycle remained higher than the starting value. This behavior is consistent with findings by Paola Marín Castaño et al. (2020), who reported irreversible aggregation and persistent clusters during cooling. Furthermore, time-dependent rheopexy was evident in the 1.5 wt% emulsion at 65 °C, where the viscosity increased from 54.87 to 58.63 mPa·s over 600 s under constant shear, confirming continued network formation even under static conditions. For the low-concentration emulsions, a subtle restructuring was noticed during cooling, but viscosity did not fully return to the initial value, indicating minor

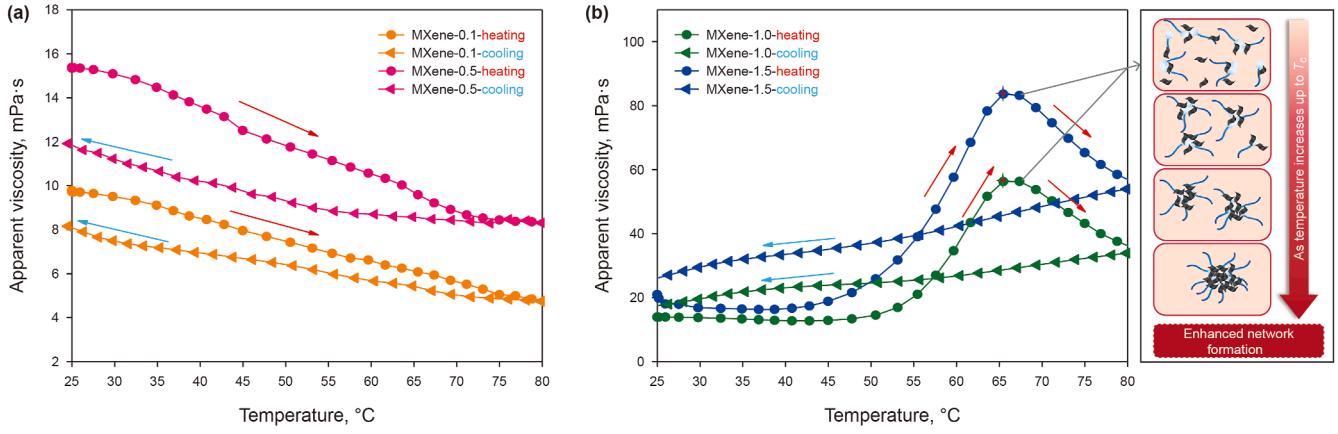

Fig. 13. Viscosity–temperature relationship of the formulated Pickering emulsions at various concentrations of DL-$Ti_3C_2T_x$ MXene: (**a**) MXene-0.1 and (**b**) MXene-1.0.

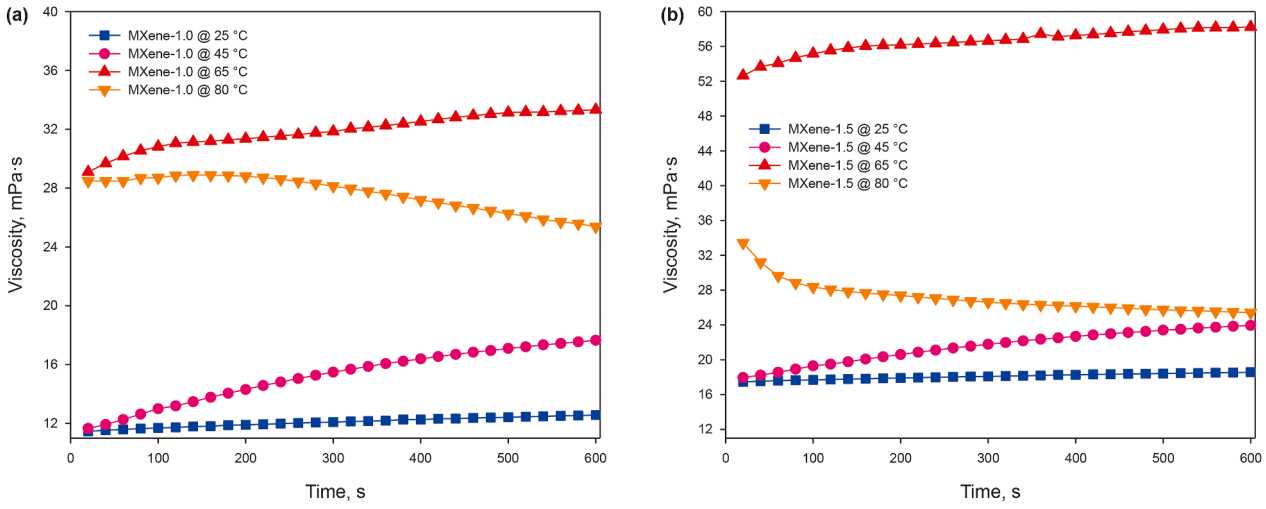

Fig. 14. Viscosity versus time curves for concentrated MXene-stabilized Pickering emulsions at different temperatures: (**a**) MXene-1.0 and (**b**) MXene-1.5.

irreversible changes. These observations are consistent with Sunny et al. (2011), where dilute nanofluids exhibited stable gel networks due to irreversible aggregation. Likewise, Lupu et al. (2023) reported hysteresis behavior in Pluronic F127 gels, where gel strength was not fully recovered after a heating–cooling cycle, reflecting persistent structural changes similar to those found here. Overall, the results indicate that higher MXene concentrations promote network formation, enhance thermal resilience, and increase the likelihood of irreversible aggregation during thermal cycles. Understanding these transitions is crucial for optimizing MXene-based systems in thermally demanding applications.

3.7.4. Temperature-dependent activation energy analysis

Understanding how temperature influences the viscosity of emulsions is crucial for predicting their behavior under varying thermal conditions, especially in oilfield applications such as EOR. In this study, the temperature–viscosity data were utilized to predict activation energy of the DL-$Ti_3C_2T_x$ MXene-stabilized Pickering emulsions using an Arrhenius-like equation:

$$\eta = A \cdot e^{E_a/RT} \tag{5}$$

where η is the apparent viscosity, mPa·s; A is the frequency factor; E_a represents the activation energy, kJ/mol; R is the universal gas constant; and T is the absolute temperature, K (Kolotova et al., 2018). Activation energy (E_a) quantifies the energy barrier needed for flow, indicating how easily molecules or particles can move past each other (Rao, 2014). The following linearized form of Eq. (5) was used to determine E_a from the slope and A from the intercept by plotting $\ln(\eta)$ versus $1/T$.

$$\ln(\eta) = \ln(A) + \frac{E_a}{R} \cdot \frac{1}{T} \tag{6}$$

For Pickering emulsions with lower MXene concentrations (MXene-0.1 and MXene-0.5), the viscosity steadily decreased with rising temperature, displaying typical temperature-thinning behavior. The Arrhenius plots in Fig. 15(a) and (b) showed good linearity, and the calculated activation energies were 11.32 and 10.61 kJ/mol, respectively (Table 2). These relatively low E_a values indicate moderate sensitivity of viscosity to temperature changes, with viscosity decreasing exponentially as temperature increases. Increasing the MXene concentration slightly reduced the activation energy, suggesting improved flow initiation and greater responsiveness to thermal or mechanical disturbances. Similar behavior has been reported in the literature. Kedar and Bhagwat (2018) found that the activation energy for crude oil emulsion destabilization decreased with increasing surfactant concentration. Pal and Mandal (2020) also observed reduced activation energy in emulsions containing partially hydrolyzed polyacrylamide (PHPA) and SiO_2 NPs stabilized with Gemini surfactants, particularly during interactions with sandstone substrates.

In contrast, Pickering emulsions with higher MXene concentrations (MXene-1.0 and MXene-1.5) exhibited nonlinear $\ln(\eta)$ versus $1/T$ relationships that deviated from typical Arrhenius behavior, as shown in Fig. 15(c) and (d). The viscosity data for these samples were therefore divided into three regions and analyzed separately (see Fig. 15(e) and (f)). The extracted values for E_a and A are presented in Table 3. In Region I (25.0–47.7 °C for MXene-1.0 and 25.0–40.7 °C for MXene-1.5), the viscosity decreased with temperature as expected, but the activation energies were much higher than those observed for the low-concentration emulsions: 36.28 kJ/mol for MXene-1.0 and 29.15 kJ/mol for MXene-1.5. These elevated values suggest stronger particle–particle interactions that require more energy to initiate flow. This could be attributed to higher reference energies and lower energy barriers between emulsion droplets (Mishchuk et al., 2004).

In Region II (47.7–67.4 °C for 1.0 wt% MXene Pickering emulsion and 40.7–65.4 °C for 1.5 wt% MXene Pickering emulsion), the viscosity anomalously increases with rising temperature, indicated by negative activation energies (−81.58 kJ/mol for 1.0 wt% MXene Pickering emulsion and −66.41 kJ/mol for 1.5 wt% MXene Pickering emulsion). For example, the 1.0 wt% Pickering emulsion viscosity increased from ~12.75 mPa·s at around 42 °C to a peak of 56.35 mPa·s at 67.0 °C. Similarly, the 1.5 wt% emulsion viscosity rose from 16.30 mPa·s at 37.0 °C to a peak of 83.63 mPa·s at 65.5 °C. This unusual increase indicates the formation of a transient network within the emulsion, likely caused by droplet flocculation. Similar trends have been observed in systems containing NPs like sterically stabilized iron oxide and alumina nanofluids, where viscosity spikes at a critical temperature due to increased van der Waals interactions and network formation (Koh et al., 2002). This gelation effect suggests that at high MXene concentrations the NPs actively participate in forming a complex internal structure, making the Pickering emulsion more resistant to flow. In Region III (67.4–80.0 °C for 1.0 wt% MXene Pickering emulsion and 65.4–80.0 °C for 1.5 wt% MXene Pickering emulsion), viscosity

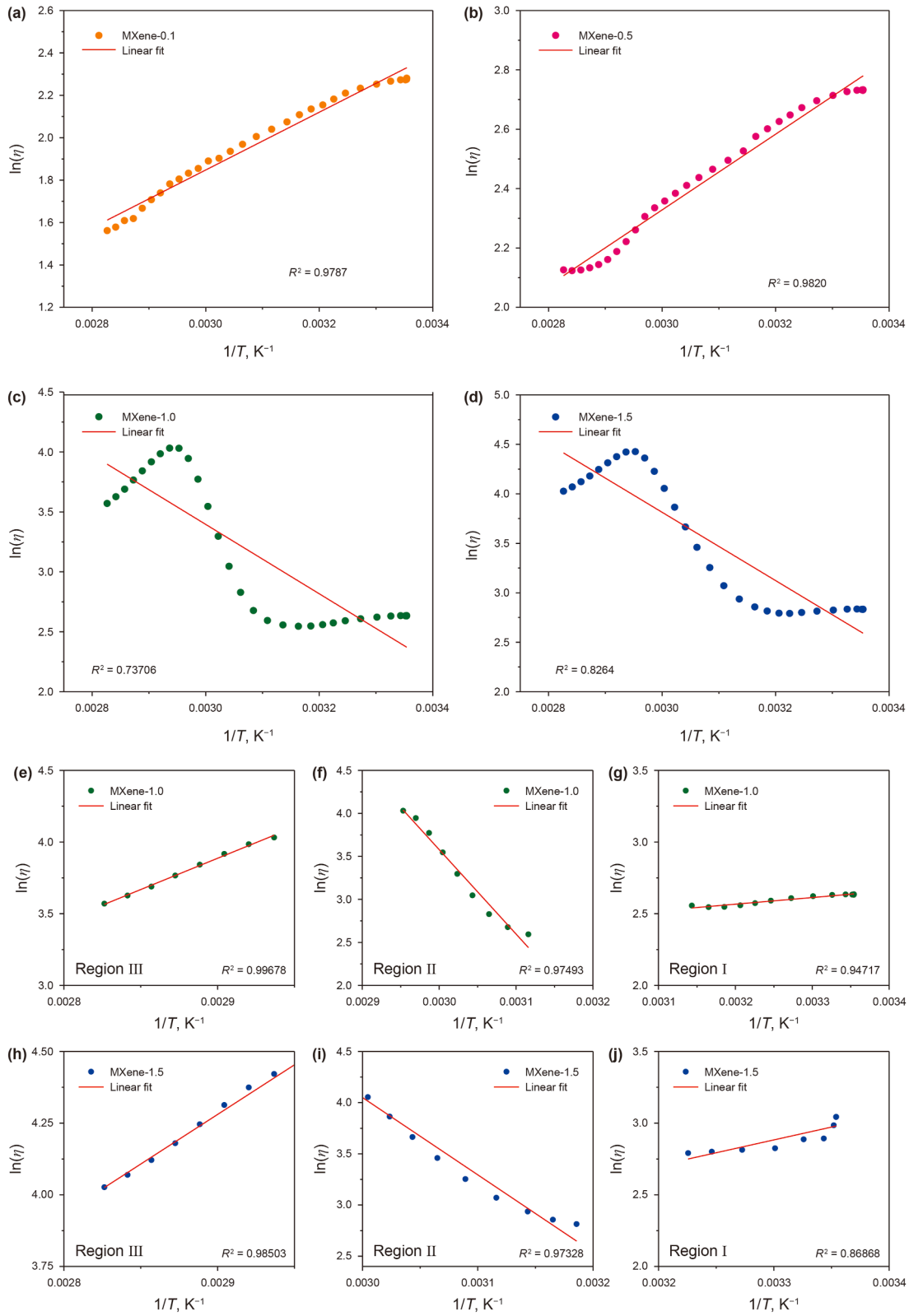

Fig. 15. Plots of ln(η) versus 1/T for Pickering emulsions containing different concentrations of MXene: (**a**) MXene-0.1, (**b**) MXene-0.5, (**c**) MXene-1.0, and (**d**) MXene-1.5. The solid lines represent Arrhenius fittings. For MXene-1.0, region-specific fittings are shown for Region III (**e**), Region II (**f**), and Region I (**g**). For MXene-1.5, region-specific fittings are shown for Region III (**h**), Region II (**i**), and Region I (**j**).

Table 2
Activation energies and pre-exponential factors for low-concentration DL-$Ti_3C_2T_x$ MXene-stabilized Pickering emulsions.

MXene concentration, wt%	E_a, kJ/mol	A, mPa·s	R^2
0.1	11.32	0.1068	0.9787
0.5	10.61	0.2200	0.9849

Table 3
Activation energies and pre-exponential factors for high-concentration DL-$Ti_3C_2T_x$ MXene-stabilized Pickering emulsions.

MXene concentration, wt%	Temperature range, °C	E_a, kJ/mol	A, mPa·s	R^2
1.0	25.0–47.7	36.28	2.00×10^{-4}	0.9968
	47.7–67.4	−81.58	2.18×10^{14}	0.9749
	67.4–80.0	3.89	2.91	0.9421
1.5	25.0–40.7	29.15	2.90×10^{-3}	0.9798
	40.7–65.4	−66.41	8.93×10^{14}	0.9394
	65.4–80.0	12.30	1.40×10^{-1}	0.9394

returns to thermal thinning behavior with positive activation energies (3.89 kJ/mol for 1.0 wt% MXene Pickering emulsion and 12.30 kJ/mol for 1.5 wt% MXene Pickering emulsion). As temperature increases further, the thermal energy becomes sufficient to disrupt the network structure formed in Region II, allowing the system to transition back to a more fluid state. This indicates that at higher temperatures, the supplied thermal energy overcomes the cohesive forces between MXene particles, resulting in a breakdown of particle aggregates (Lupu et al., 2023). Similar observation was reported elsewhere for Pluronic F127 gels with added ZnO NPs, where increasing temperature initially strengthened the gel, but beyond a critical point, the gel structure began to break down (Koh et al., 2002).

The non-Arrhenius behavior observed at higher MXene concentrations highlights the significant impact of temperature-induced structural changes. Similar trends have been reported in nanofluids, where gelation and network formation dramatically alter flow characteristics at critical temperatures (Koh et al., 2002). Understanding these complex rheological behaviors is crucial for designing Pickering emulsions that maintain their integrity and flow properties under varying thermal conditions, ensuring stability and efficiency in EOR processes.

3.8. Rheological modeling of emulsion flow properties

Modeling analysis was performed to identify the best-fit model for describing the rheological behavior of the Pickering emulsions at different temperatures (25, 45, and 65 °C). Three widely used rheological models the Bingham equation, Ostwald–de Waele model, and Herschel–Bulkley model were applied, as given in Table 4. These models are particularly effective in capturing the complex flow properties of colloidal suspensions like Pickering emulsions (Ariffin et al., 2016). The experimental shear stress versus shear rate data at 25 °C were fitted to these models, with the results summarized in Table 4 (Results for 45 and 65 °C are provided Tables A1 and A2 in Appendix A). To visually compare the model fits, Fig. 16 presents the shear stress-shear rate curves for the Pickering emulsions at 25 °C (Figures related to 45 and 65 °C are provided in Figs. A1 and A2 in Appendix A).

Among the three models, the Herschel–Bulkley model provided the best fit, capturing both the yield stress and non-Newtonian behavior of the Pickering emulsions, particularly at higher MXene concentrations. The flow behavior index (n) obtained from the Herschel–Bulkley model effectively characterizes the type of flow exhibited by each emulsion. For the 0.1 wt% MXene Pickering emulsion, Newtonian behavior was observed, as indicated by a flow behavior index n close to 1 ($n \approx 1.03$), with negligible yield stress. This suggests that the MXene nanosheets were well-dispersed, resulting in a smooth, easy-flowing emulsion with constant viscosity. However, as the concentration increased to 0.5 wt%, the Pickering emulsion began to display slight shear-thinning behavior, with a flow behavior index n of ~0.91 and a small yield stress. This points to the onset of particle–particle interactions, which create a weak network structure that resists flow until a certain stress threshold is reached. At higher concentrations of 1.0 and 1.5 wt% MXene, the Pickering emulsions exhibited strongly non-Newtonian behavior, with flow behavior indices dropping further ($n \approx 0.79$ and $n \approx 0.55$, respectively), and yield stress increasing significantly. This suggests the development of a more robust internal structure within the Pickering emulsions, possibly forming gel-like networks due to enhanced particle aggregation and interparticle interactions. The same modeling analyses were extended to higher temperatures of 45 and 65 °C (see the supplementary materials), revealing similar trends and confirming the impact of MXene concentration on the overall rheological properties.

To further illustrate the influence of temperature, the K_{HB} and n from the Herschel–Bulkley model were plotted against temperature for each MXene concentration, as shown in Fig. 17. Fig. 17(a) highlights the changes in K_{HB} with temperature for different MXene concentrations. At lower concentrations, the steady decline in K_{HB} reflects thermal thinning due to the reduced viscosity of the continuous phase. However, at higher concentrations, the initial decrease followed by a slight increase in K_{HB} suggests that temperature might be enhancing particle–particle interactions, leading to stronger network formation despite the overall thermal thinning. Fig. 17(b) illustrates the effect of temperature on the n for different MXene concentrations. For the 0.1 wt% MXene Pickering emulsion, the consistent Newtonian behavior (n is close to 1) indicates that temperature has a minimal effect on n at low MXene concentrations. However, at higher concentrations, the trend of n with temperature becomes more complex. An increase in n at moderate temperatures suggests a partial disruption of the particle networks, resulting in reduced shear-thinning. Conversely, a decrease in n at elevated temperatures points to enhanced aggregation and stronger network formation, leading to more pronounced shear-thinning behavior. This dynamic interplay between

Table 4
Rheological parameters for DL-$Ti_3C_2T_x$ MXene-stabilized Pickering emulsions at 25 °C.

Pickering emulsion concentration	Ostwald–de Waele model $\tau = k_{OW}\cdot\gamma^n$			Bingham model $\tau = \tau_0 + \eta_B\cdot\gamma$			Herschel–Bulkley model $\tau = \tau_0 + K_{HB}\cdot\gamma^n$			
	n	k_{OW}, mPa·s^n	R^2	τ_0, mPa	η_B, mPa·s	R^2	τ_0, mPa	K_{HB}, mPa·s	n	R^2
MXene-0.1	1.02111±0.00236	6.90±0.10	0.99994	6.53±3.93	7.87±0.02	0.99981	9.79±2.19	6.60±0.10	1.02801±0.00243	0.99997
MXene-0.5	0.88493±0.00768	19.59±0.89	0.99899	104.93±14.59	9.56±0.08	0.99740	36.62±11.43	16.98±1.03	0.90701±0.00982	0.99922
MXene-1.0	0.78085±0.0058	57.61±2.00	0.99932	335.77±54.46	14.33±0.27	0.98901	36.19±20.51	53.57±2.87	0.79182±0.00844	0.99938
MXene-1.5	0.51942±0.00621	494.41±17.14	0.99734	1722.57±175.67	23.88±0.99	0.94290	227.12±85.17	409.97±32.64	0.54765±0.01243	0.99776

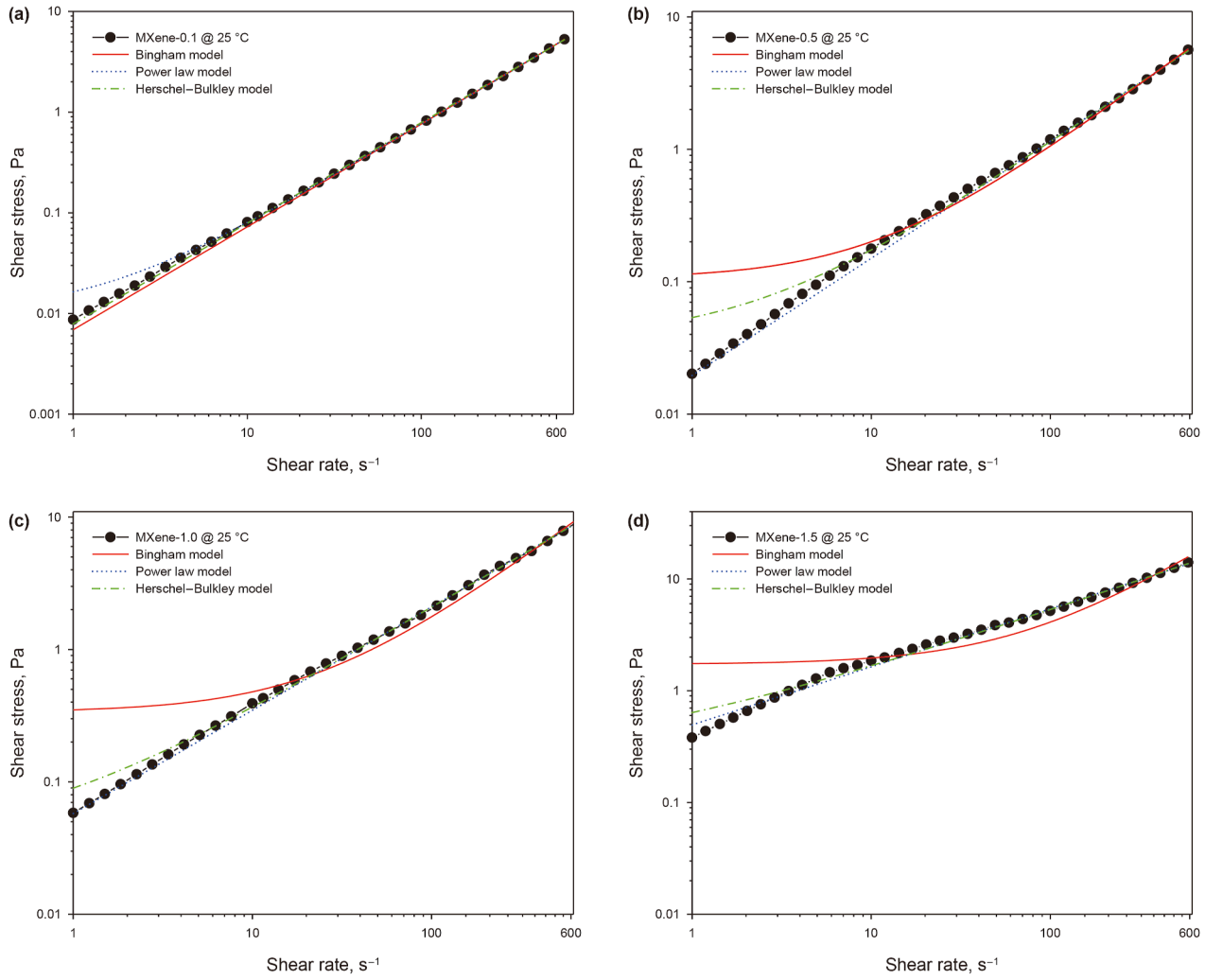

Fig. 16. Shear stress versus shear rate curves for DL-$Ti_3C_2T_x$ MXene-stabilized Pickering emulsions at 25 °C, highlighting the comparison of model fits. Panels show results for different MXene concentrations: (**a**) MXene-0.1, (**b**) MXene-0.5, (**c**) MXene-1.0, and (**d**) MXene-1.5.

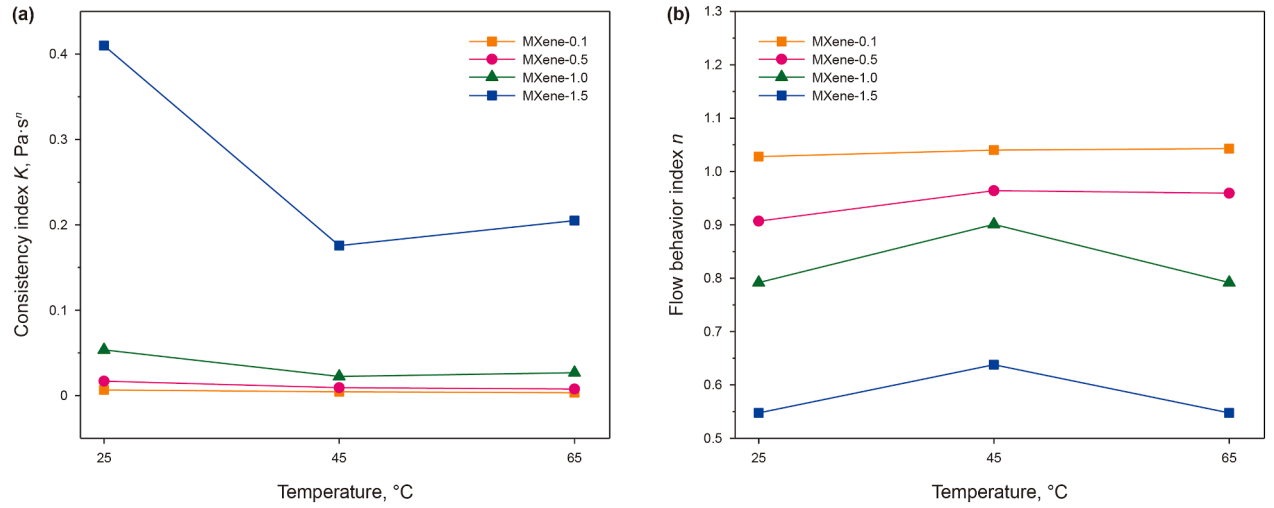

Fig. 17. (**a**) Variation of K_{HB} with temperature for DL-$Ti_3C_2T_x$ MXene-stabilized Pickering emulsions, illustrating the influence of temperature on the rheological parameters derived from the Herschel–Bulkley model. (**b**) Variation of n with temperature for emulsions containing different MXene concentrations.

temperature and particle concentration highlights the importance of tuning both parameters to achieve the desired rheological properties of DL-$Ti_3C_2T_x$ MXene-stabilized Pickering emulsions.

3.9. Comparative evaluation of emulsifying systems

Pickering emulsions have been extensively studied across various applications including EOR, pollutant remediation, drug delivery, and encapsulation (Abu Zaid et al., 2024). A commonly observed trend is the superior emulsion stability achieved by combining nanoparticles with surfactants. However, the extent and persistence of this synergistic behavior depend strongly on the nanoparticle type, surface modification, and surfactant structure. For instance, SiO_2-based emulsifiers dominate many reports and include unmodified silica (Xu et al., 2017), amphiphilic SiO_2 modified with alkylsilanes (Wang et al., 2024), Janus SiO_2 (Xu et al., 2023), and SiO_2 coated with active agents such as ALS and SOS (Tliba et al., 2025). Metal oxide systems like ZnO coupled with rhamnolipid and sophorolipid biosurfactants have also been proposed for crude oil emulsification (Gazem et al., 2025b). Some studies employed functionalized MXenes such as PEGylated $Ti_3C_2T_x$ (He et al., 2024), which required surface treatments to enhance dispersion or interfacial reactivity. A range of surfactants have been paired with these nanoparticles, including non-ionic agents like Tween 60 and C12E5, ionic types such as SDS and SDBS, and natural biosurfactants. Each pairing influences droplet size, zeta potential, IFT, and demulsification behavior, as summarized in Table 5.

In comparison, the DL-$Ti_3C_2T_x$ MXene-Tween 40 system developed in this study shows clear advantages in physical stability, simplicity, and interfacial characteristics. At 0.5 wt% MXene, the system achieved a low IFT of 2.42 mN/m, a zeta potential of −47.70 mV, and a droplet size of 5.02 μm. These values reflect strong interfacial packing and electrostatic stabilization. After 24 h, the emulsions maintained exceptionally low separation values across all concentrations: 0 at 0.1 wt%, 0 at 0.5 wt%, 0.6% at 1.0 wt%, and 1.0% at 1.5 wt%. These results compare favorably with other systems. For example, the OP-50/SiO_2 emulsions reported by Wang et al. (2024) showed ~23% phase separation after 24 h, despite being described as highly stable. Janus SiO_2 paired with SDS/Tween 60 at 0.02 wt% led to 40%–60% separation at 24 h, depending on NP concentration (Xu et al., 2023). PEGylated MXene emulsions (0.3 mg/mL) with SDBS (3 mg/mL) showed 35.8% separation within 24 h (He et al., 2024). Even ZnO-based emulsions stabilized with 2000 ppm of mixed biosurfactants showed turbidity and initial instability by day 7 (Gazem et al., 2025b). By contrast, our MXene emulsions maintained complete physical integrity at 24 h without the need for functionalization or high surfactant loading.

Longer-term performance further distinguishes the MXene-Tween 40 system. Over a 30-d period, phase separation remained modest, with DI values rising gradually to 13% for 0.1 wt%, 17% for 0.5 wt%, 20% for 1.0 wt%, and 25% for 1.5 wt%. In contrast, many literature systems either lack long-term data or show significantly higher separation over shorter durations. For instance, the $C_{12}E_5/SiO_2$ emulsions separated completely within 10–45 min under mild heating (Zhu et al., 2017), while ALS/SOS emulsions showed 20%–23% separation after two weeks, even at higher NP concentrations (Tliba et al., 2025). Although the SiO_2@ALS and SiO_2@SOS systems achieved low IFT values below 2 mN/m, they still exhibited 5%–13% separation within two weeks, depending on formulation. In our case, even at 1.5 wt% MXene where aggregation increased and zeta potential dropped to −37.06 mV, the emulsion retained superior short- and long-term stability. This confirms that despite mild drawbacks such as increased droplet size at higher NP concentrations, the emulsions preserved functional performance beyond what is typically observed for over-concentrated NP systems.

Additionally, our system's practical simplicity and responsiveness-free stability offer further merit. Unlike many responsive emulsions that require triggers like heat or voltage to recover or maintain stability (Yu et al., 2019), the DL-$Ti_3C_2T_x$-Tween 40 emulsions remained stable at ambient conditions. Emulsification and demulsification occurred without relying on functional groups, electrical input, or tailored pH and temperature environments. Compared to other materials, our MXene-Tween 40 system avoids the need for surface modification or external triggers. For example, PEGylated MXene ($Ti_3C_2T_x$-PEG) used with SDBS showed rapid destabilization, with 35.8% separation in just 24 h (He et al., 2024). Similarly, $C_{12}E_5/SiO_2$ systems (Zhu et al., 2017) displayed full separation within 10–45 min under mild heating, even though they were stable at room temperature. SiO_2-FcCOC10N systems required surfactant concentrations of up to 3.0 mmol/L to achieve droplet sizes near 28 μm, with initial sizes exceeding 400 μm. The droplet size reduction occurred with increasing surfactant content, yet even at optimal conditions, their droplets remained significantly larger than those observed in our formulation. Zhu et al. (2017) also reported droplet sizes of ~400 μm even at 1 mmol/L $C_{12}E_5$, which decreased slightly upon thermal cycling but still remained substantially larger than our system. Many responsive Pickering emulsions require either chemical modification or controlled triggers such as heating or applied voltage to recover or maintain stability, as in the case of electrically switchable systems (i.e., emulsification/demulsification or responsive Pickering emulsions). In addition to offering low IFT and small droplet sizes across concentrations, our emulsions achieved one of the highest known combinations of electrostatic repulsion, interfacial packing, and long-term physical resistance using only unmodified 2D MXene and a non-ionic surfactant. These results position our formulation as a highly promising and practical candidate for field-scale application in Pickering emulsion systems.

Overall, this comparative evaluation demonstrates that the DL-$Ti_3C_2T_x$ MXene-Tween 40 system not only matches but often exceeds the performance of more complex nanoparticle–surfactant emulsions reported in the literature. Its ability to achieve low interfacial tension, fine droplet size, and extended phase stability without relying on chemical modifications, responsive stimuli, or high surfactant loadings highlights its practical strengths. These findings support its potential as a robust and scalable candidate for applications requiring emulsion integrity, operational simplicity, and long-term stability, particularly in challenging environments such as EOR.

Table 5
Comparison of nanoparticle–surfactant stabilized Pickering emulsions from literature.

Surfactant name	NP name	Oil name	Oil/water ratio	Emulsion type	IFT, mN/m	Phase separation	Zeta potential, mV	Droplet size, μm	Performance summary	References
Tween 40 (0.5 wt%)	DL-$Ti_3C_2T_x$ MXene (0.1 wt%)	Diesel	1:1	O/W	3.01	0, 4.0%, 8.0%, 13.0% for 1, 10, 20, and 30 d	−49.76	3.43	Highly stable; minimal aggregation; fine droplets	This study
Tween 40 (0.5 wt%)	DL-$Ti_3C_2T_x$ MXene (0.5 wt%)	Diesel	1:1	O/W	2.42	0, 5.4%, 11.4%, 17.0% for 1, 10, 20, and 30 d	−47.70	5.02	Moderate stability; initial signs of aggregation	This study
Tween 40 (0.5 wt%)	DL-$Ti_3C_2T_x$ MXene (1.0 wt%)	Diesel	1:1	O/W	1.58	0.6%, 8.0%, 11.8%, 20.0% for 1, 10, 20, and 30 d	−43.71	7.16	Aggregation apparent; reduced interfacial coverage	This study
Tween 40 (0.5 wt%)	DL-$Ti_3C_2T_x$ MXene (1.5 wt%)	Diesel	1:1	O/W	0.86	1.0%, 10.0%, 15.8%, 25.0% for 1, 10, 20, and 30 d	−37.06	16.39	Significant aggregation; poor dispersion and stability	This study
OP-50 (0.1 wt%)	Amphiphilic SiO_2 modified with C_8 (*n*-octyltriethoxysilane, 10:1)	Kerosene	1:1	O/W	~6.3	~23% (after 24 h)	–		Best stability among all NP-surfactant systems; strongest interfacial film	Wang et al. (2024)
FcCOC10N (redox-responsive cationic surfactant) (0.01–3.0 mmol/L)	SiO_2 (0.5 wt%)	Isooctane, toluene, *n*-octane	1:1	O/W	~40.78 (reduced form), ~60.49 (oxidized form)	Stable for > 1 month; full demulsification achieved within 2 h under 0.8 V; re-emulsified upon reduction and homogenization	−25.4 to +34.5 (increased with FcCOC10N)	Decreased from 432 to 28 μm with increasing FcCOC10N	Highly stable, electrically switchable Pickering emulsions formed at ultra-low surfactant concentration (0.005 CMC); emulsifier system is recyclable and environmentally benign	Yu et al. (2019)
Pentaethylene glycol monododecyl ether ($C_{12}E_5$) (0.01–1.0 mmol/L)	SiO_2 (0.5 wt%)	Toluene	1:1	O/W	7.1±0.6 → 5.6±0.1 (after 2 cycles)	Stable for ≥ 3 months at 22 °C; 100% separation after 10–45 min at 45 °C with stirring	−25.6±0.3	~400 at 0.06 mmol/L → ~50–100 at 1 mmol/L	Thermoresponsive Pickering emulsions. Stable at room temperature; reversible demulsification on heating; improved IFT and droplet size with cycling.	Zhu et al. (2017)
ALS	–	Algerian dead crude oil (API 24.6, 71 cP at 25 °C)	1:9	O/W	~10–13 at 100–500 ppm, limited reduction at low ppm	~22%–23% at 100–1000 ppm (after 2 weeks)	–		Moderate IFT reduction at high dose; poor stability at low concentration; requires ≥ 500 ppm for effective use.	Tliba et al. (2025)
ALS	ALS-NPs (SiO_2@ALS)	Algerian dead crude oil (API 24.6, 71 cP at 25 °C)	1:9	O/W	< 2 at 50 ppm, < 1 at 100 ppm, 10^{-2}–10^{-4} with 0.1 wt% alkali	~5% at 50 ppm, ~9% at 100 ppm (after 2 weeks)	−46 (no alkali), −56 (with alkali)		Excellent IFT reduction and stability at low concentration;	Tliba et al. (2025)

(*continued on next page*)

Table 5 (*continued*)

Surfactant name	NP name	Oil name	Oil/water ratio	Emulsion type	IFT, mN/m	Phase separation	Zeta potential, mV	Droplet size, μm	Performance summary	References
									alters wettability; strong dual-action for EOR.	
SOS	–	Algerian dead crude oil (API 24.6, 71 cP at 25 °C)	1:9	O/W	~9–11 at 100–500 ppm. Limited reduction at low ppm	~20%–21% at 100–1000 ppm (after 2 weeks)	–		Good reduction at higher dose; moderate emulsion stability; less effective below 100 ppm.	Tliba et al. (2025)
SOS	SOS-NPs (SiO_2@SOS)	Algerian dead crude oil (API 24.6, 71 cP at 25 °C)	1:9	O/W	< 2 at 50 ppm, < 1 at 100 ppm, 10^{-2}–10^{-4} with 0.1 wt% alkali	~10% at 50 ppm, ~13% at 100 ppm (after 2 weeks)	−40 (no alkali), −50 (with alkali)		High performance at low dose; strong IFT reduction and stability; more effective than SOS alone.	Tliba et al. (2025)
Tween 40 (0.05 wt%)	SiO_2 NP (2%)	Decane	0.192, 0.333, 0.385	O/W	9.1	–	–	100–400	Excellent synergistic stability. High maximum oil saturation achieved. Lamella-like droplet packing and strong resistance to coalescence. Superior matrix sweep and blockage of high-permeability paths.	Xu et al. (2017)
M. neoaurum cells (40 g/L)	SiO_2-OTS(20), 1–5 g/L	Bis(2-ethylhexyl) phthalate	1:2	W/O → O/W (inversion at 3 g/L)	–	Max ~82% at 3 g/L	–	> 100 μm at inversion; reduced after	Addition of moderately hydrophobic silica induced phase inversion and droplet coalescence. Max dewatering at 3 g/L; larger droplets formed around inversion point; confirms competitive adsorption and destabilization.	Xie et al. (2022)
M. neoaurum cells (40 g/L)	SiO_2-OTS(30), 0.5–3 g/L	Bis(2-ethylhexyl) phthalate	1:2	W/O → O/W (inversion at 1.25 g/L)	–	Max ~87% at 1.5 g/L	–	> 100 μm at inversion; then decreased	Stronger hydrophobicity led to lower required concentration for inversion; optimal demulsification at 1.5 g/L. CLSM confirmed silica displaced bacteria at interface; coalescence and creaming observed.	Xie et al. (2022)

M. neoaurum cells (70 g/L)	SiO_2-OTS(30), 0–3 g/L	Bis(2-ethylhexyl) phthalate	1:4	W/O → O/W (inversion at 1.5 g/L)	–	Max 87% at 1.5 g/L	–	–	During microbial transformation emulsion, silica successfully enabled product recovery. Dewatering allowed downstream methanol extraction without surfactant. > 95% BEHP recovered, > 84% AD + ADD yield achieved.	Xie et al. (2022)
SDBS (3 mg/mL)	$Ti_3C_2T_x$-COOH-g-PEG (0.3 mg/mL)	Crude oil	1:1	W/O	0.08–0.18 (0–20000 ppm NaCl)	4.7% (10 min), 10.0% (30 min), 15.0% (1 h), 27.9% (6 h), 35.5% (12 h), 35.8% (24 h)	–	–	High viscosity and interfacial activity under salinity, temperature, and pH variations.	He et al. (2024)
SDS/Tween 60 (3:7 molar ratio, 0.02 wt%)	Janus SiO_2 (0.005 wt%)	Crude oil	–	O/W	~3.30	High (~60%)	–	~0.07	Least stable emulsion; moderate IFT drop; recovery increased by 3.7%	Xu et al. (2023)
SDS/Tween 60 (3:7 molar ratio, 0.02 wt%)	Janus SiO_2 (0.01 wt%)	Crude oil	–	O/W	~2.40	Moderate (~40 %)	–	~0.10	Best emulsion stability and highest EOR; recovery increased by 15.3%	Xu et al. (2023)
SDS/Tween 60 (3:7 molar ratio, 0.02 wt%)	Janus SiO_2 (0.02 wt%)	Crude oil	–	O/W	1.49	Slightly higher (~45%)	–	~0.15	Lowest IFT; slightly less stable; recovery increased by 11.1%	Xu et al. (2023)
Rhamnolipid 2000 ppm + sophorolipid 2000 ppm	ZnO (500 ppm)	Panna-Mukta crude oil	–	–	~26.2 at 30 °C	Slight turbidity at day 7	−27.3	~0.15	Good stability; narrow droplet distribution; best zeta potential; moderate IFT reduction; recovery ~87.81%	Gazem et al. (2025b)
Rhamnolipid 2000 ppm + sophorolipid 2000 ppm	ZnO (1000 ppm)	Panna-Mukta crude oil	–	–	~26.4 at 30 °C	Turbid but stable at day 7	−23.7	~0.20	Stable; some droplet size decreases over 7 d; moderate zeta; slight IFT increase at 70 °C; recovery ~91.19%	Gazem et al. (2025b)
Rhamnolipid 2000 ppm + sophorolipid 2000 ppm	ZnO (2000 ppm)	Panna-Mukta crude oil	–	–	~25.8 at 30 °C	Most stable, uniform turbidity at day 7	−22.0	~0.20	Best performance; very stable colloids; good zeta; lowest IFT; strong wettability alteration (CA = 27.3°); best recovery (95.14% OOIP)	Gazem et al. (2025b)

4. Conclusions

This study successfully formulated and evaluated diesel-in-water Pickering emulsions stabilized by DL-$Ti_3C_2T_x$ MXene in combination with Tween 40, demonstrating the synergistic effect of nanoparticle–surfactant interactions in achieving enhanced emulsion stability. The hybrid emulsions exhibited excellent kinetic and long-term stability, with no phase separation observed at 0.1 and 0.5 wt% MXene after 24 h, while emulsions with 1.0 and 1.5 wt% showed limited separation of 2% and 6%, respectively. While the MXene-only system failed to form stable emulsions, and the surfactant-only system achieved lower stability, the hybrid formulation significantly outperformed both. These findings highlight the complementary roles of MXene nanosheets, which provide interfacial adsorption and rigidity, and Tween 40, which supplies steric stabilization and prevents coalescence. The Pickering emulsions demonstrated robustness under various thermal and mechanical conditions, showing adaptability for demanding applications such as EOR. The combination of MXene and Tween 40 not only improved emulsion stability but also enhanced interfacial tension reduction and facilitated the transition to shear-thinning behavior at higher MXene concentrations. These features are particularly valuable in oilfield operations where flow control and emulsion integrity are critical. Rheological analysis, supported by models such as Ostwald–de Waele, Bingham, and Herschel–Bulkley, provided a comprehensive understanding of the emulsion's flow behavior, further confirming their suitability for industrial applications. To the best of our knowledge, this is the first demonstration of stable diesel-in-water Pickering emulsions prepared using pristine $Ti_3C_2T_x$ MXene for oilfield use. The combined performance improvements in interfacial tension reduction, droplet uniformity, and structural adaptability reinforce the promise of MXene-Tween 40 hybrid emulsions as a viable and surfactant-lean platform for enhanced oil recovery. While the experimental conditions do not fully replicate reservoir environments, the results underscore the system's potential for broader application. Future research may explore optimization under field-relevant salinity, pressure, and flow conditions, as well as expansion into other industrial domains. This work adds to the growing body of knowledge on MXene-based colloidal systems and their role in addressing operational and economic challenges in oilfield engineering.

CRediT authorship contribution statement

Nansee S.K. Abu Zaid: Writing – original draft, Visualization, Investigation, Formal analysis, Data curation, Conceptualization. **Aaminah Johar:** Writing – original draft, Investigation, Formal analysis, Data curation. **Mustafa S. Nasser:** Writing – review & editing, Supervision, Resources, Project administration, Data curation, Conceptualization. **Khaled A. Mahmoud:** Writing – review & editing, Supervision, Resources, Formal analysis, Conceptualization. **Sagheer A. Onaizi:** Writing – review & editing, Supervision, Resources, Project administration.

Declaration of competing interest

The authors declare that they have no known competing financial interests or personal relationships that could have appeared to influence the work reported in this paper.

Acknowledgments

This work was made possible by the support of the Qatar National Research Fund (QNRF), grant reference number GSRA9-L-2-0511-22005. The statements made herein are solely the responsibility of the authors. The authors also acknowledge M. Pasha of QEERI Core Labs for assistance with SEM measurements.

Appendix A. Supplementary data: Rheological parameters of models and correlation coefficients of mxene Pickering emulsion systems

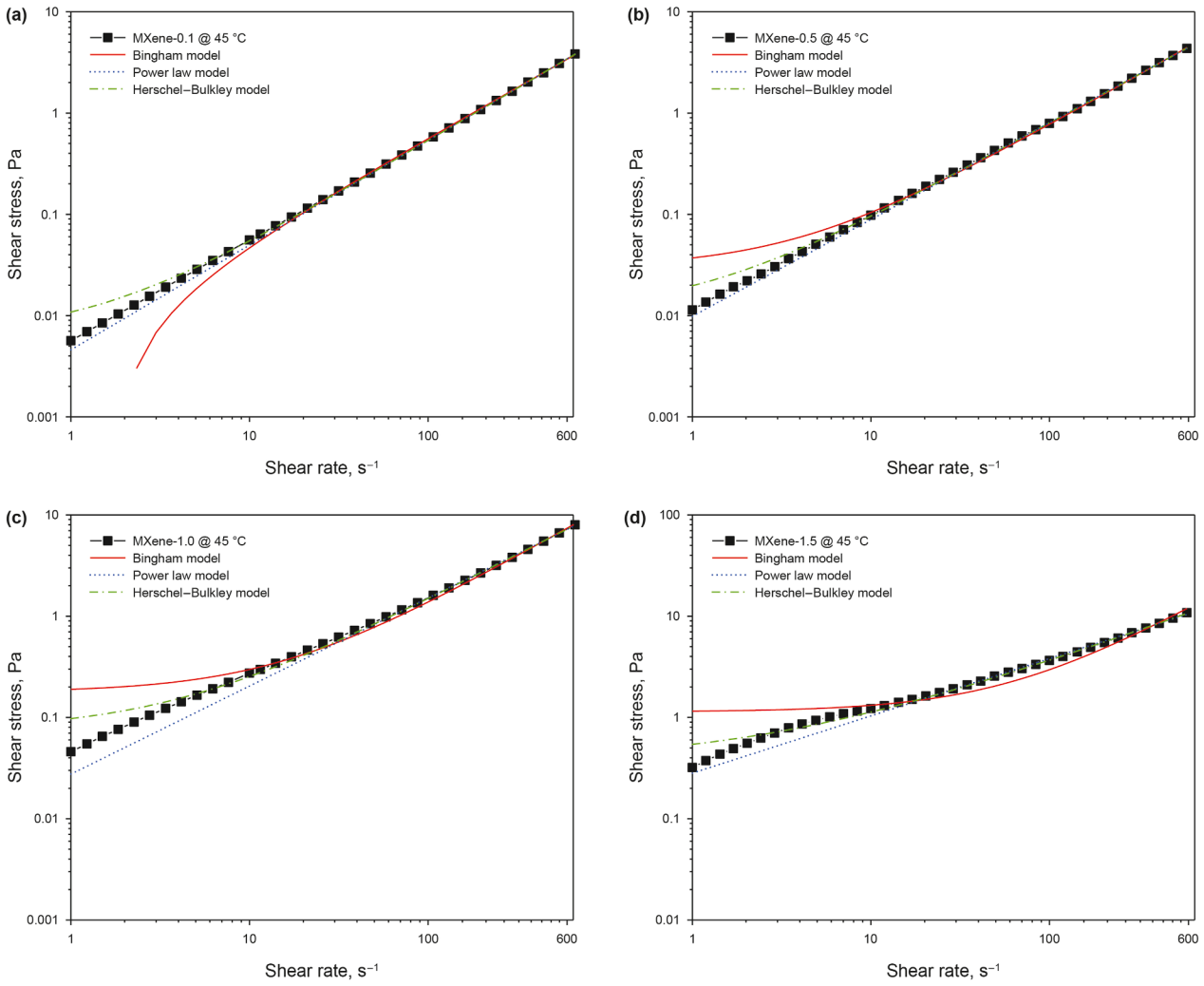

Fig. A1. Shear stress versus shear rate curves for DL-$Ti_3C_2T_x$ MXene-stabilized Pickering emulsions at 45 °C, highlighting the comparison of model fits. Panels show results for different MXene concentrations: (**a**) MXene-0.1, (**b**) MXene-0.5, (**c**) MXene-1.0, and (**d**) MXene-1.5.

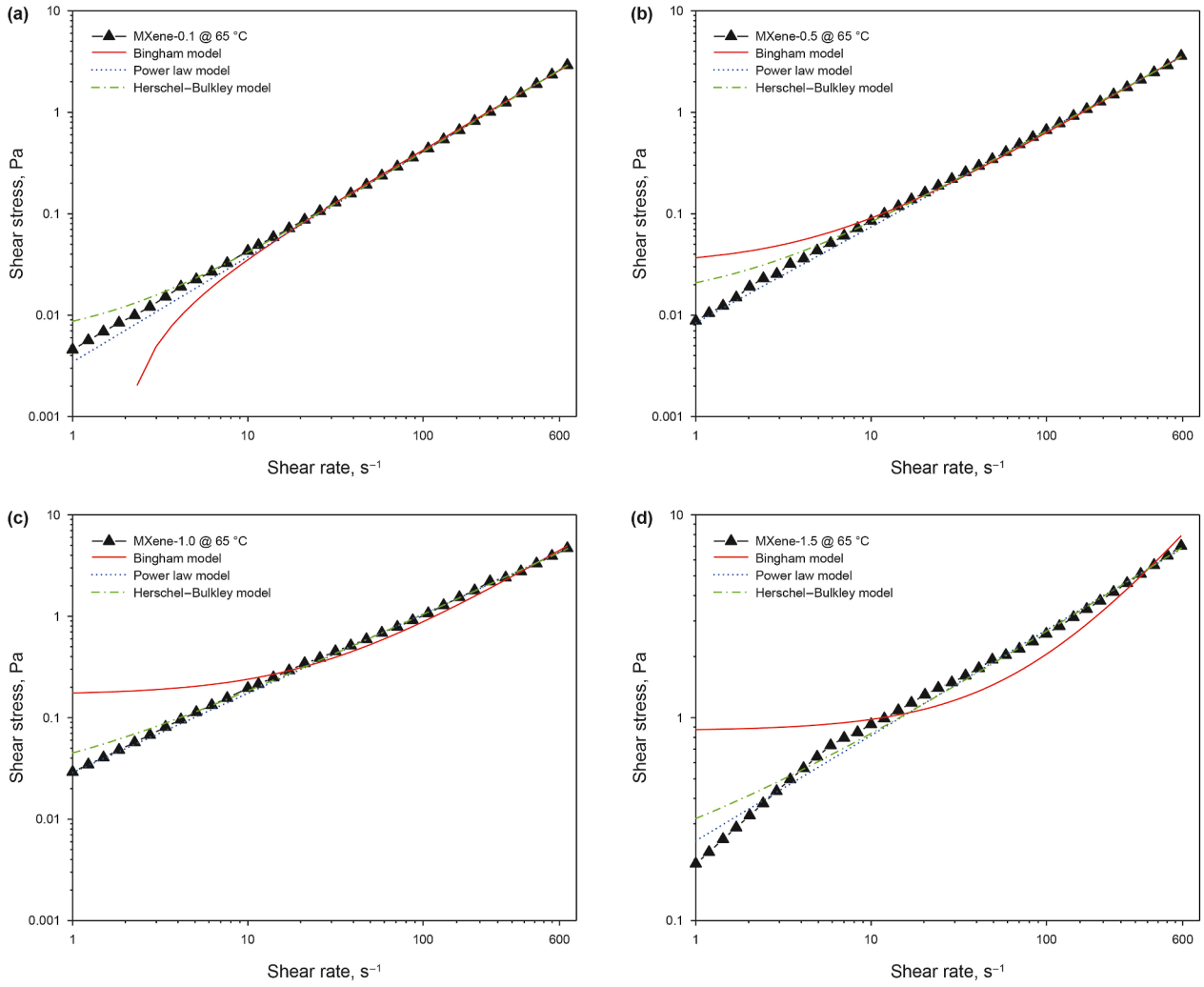

Fig. A2. Shear stress versus shear rate curves for DL-$Ti_3C_2T_x$ MXene-stabilized Pickering emulsions at 65 °C, highlighting the comparison of model fits. Panels show results for different MXene concentrations: (**a**) MXene-0.1, (**b**) MXene-0.5, (**c**) MXene-1.0, and (**d**) MXene-1.5.

Table A1
Rheological parameters for DL-$Ti_3C_2T_x$ MXene-stabilized Pickering emulsions at 45 °C.

Pickering emulsion concentration	Ostwald–de Waele model $\tau = k_{OW}\cdot\gamma^n$			Bingham model $\tau = \tau_0 + \eta_B\cdot\gamma$			Herschel–Bulkley model $\tau = \tau_0 + K_{HB}\cdot\gamma^n$			
	n	k_{OW}, mPa·s^n	R^2	τ_0, mPa	η_B, mPa·s	R^2	τ_0, mPa	K_{HB}, mPa·s	n	R^2
MXene-0.1	1.03382±0.00218	4.59±0.06	0.99995	10.21±3.82	5.67±0.02	0.99965	6.43±1.41	4.41±0.06	1.04017±0.00221	0.99997
MXene-0.5	0.9557±0.00388	9.84±0.23	0.99979	29.62±4.73	7.47±0.03	0.99955	10.37±4.06	9.33±0.28	0.96401±0.00489	0.99982
MXene-1.0	0.86993±0.00693	27.57±1.16	0.99925	177.74±21.28	12.02±0.11	0.99759	75.02±10.34	22.46±0.88	0.90098±0.00621	0.99972
MXene-1.5	0.56557±0.00824	282.12±13.14	0.99618	1135.67±104.14	18.29±0.59	0.96502	367.16±38.64	175.67±10.76	0.63793±0.00972	0.99881

Table A2
Rheological parameters for DL-$Ti_3C_2T_x$ MXene-stabilized Pickering emulsions at 65 °C.

Pickering emulsion concentration	Ostwald–de Waele model $\tau = k_{OW}\cdot\gamma^n$			Bingham model $\tau = \tau_0 + \eta_B\cdot\gamma$			Herschel–Bulkley model $\tau = \tau_0 + K_{HB}\cdot\gamma^n$			
	n	k_{OW}, mPa·s^n	R^2	τ_0, mPa	η_B, mPa·s	R^2	τ_0, mPa	K_{HB}, mPa·s	n	R^2
MXene-0.1	1.03572±0.0021	3.45±0.044	0.99996	8.03±3.04	4.32±0.02	0.99962	5.40±0.91	3.30±0.04	1.04274±0.00187	0.99998
MXene-0.5	0.94603±0.00625	8.39±0.31	0.99944	30.75±5.14	5.99±0.03	0.99918	13.18±5.39	7.71±0.38	0.95928±0.00803	0.99952
MXene-1.0	0.78083±0.00658	28.81±1.14	0.99912	167.90±27.47	7.16±0.14	0.98881	18.10±11.77	26.79±1.65	0.79181±0.00969	0.99918
MXene-1.5	0.51942±0.00621	247.20±8.57	0.99734	861.28±87.84	11.94±0.50	0.9429	113.56±42.59	204.98±16.32	0.54765±0.01243	0.99776

References

Abu Zaid, N.S.K., Johar, A., Nasser, M.S., Onaizi, S.A., 2025. Synergistic effect of chemical and bio-based surfactants in stabilizing nanoemulsions. Geoenergy Sci. Eng. 247, 213663. https://doi.org/10.1016/j.geoen.2025.213663.

Abu Zaid, N.S.K., Nasser, M.S., Onaizi, S.A., 2024. Pickering emulsions stabilized by metal-organic frameworks, graphene-based materials, and carbon nanotubes: A comprehensive review. J. Mol. Liq. 393, 123617. https://doi.org/10.1016/j.molliq.2023.123617.

Adil, M., Onaizi, S.A., 2022. Pickering nanoemulsions and their mechanisms in enhancing oil recovery: A comprehensive review. Fuel 319, 123667. https://doi.org/10.1016/j.fuel.2022.123667.

Ahmed, B., Hossain, M.J., Al Parvez, A., et al., 2024. Recent advancements of MXene/nanocellulose-based hydrogel and aerogel: A review. Adv. Energy Sustain. Res. 5 (3), 2300231. https://doi.org/10.1002/aesr.202300231.

Alhabeb, M., Maleski, K., Anasori, B., et al., 2017. Guidelines for synthesis and processing of two-dimensional titanium carbide ($Ti_3C_2T_x$ MXene). Chem. Mater. 29 (18), 7633–7644. https://doi.org/10.1021/acs.chemmater.7b02847.

Ali, S., Raza, A., Afzal, A.M., et al., 2022. Recent advances in 2D-MXene based nanocomposites for optoelectronics. Adv. Mater. Interfac. 9 (31), 2200556. https://doi.org/10.1002/admi.202200556.

Ariffin, T.S.T., Yahya, E., Husin, H., 2016. The rheology of light crude oil and water-in-oil emulsion. Procedia Eng. 148, 1149–1155. https://doi.org/10.1016/j.proeng.2016.06.614.

Behera, U.S., Poddar, S., Deshmukh, M.P., et al., 2024. Comprehensive review on the role of nanoparticles and nanofluids in chemical enhanced oil recovery: Interfacial phenomenon, compatibility, scalability, and economic viability. Energy & Fuels. https://doi.org/10.1021/acs.energyfuels.4c02248.

Blijdenstein, T.B.J., Veerman, C., van der Linden, E., 2004. Depletion–flocculation in oil-in-water emulsions using fibrillar protein assemblies. Langmuir 20 (12), 4881–4884. https://doi.org/10.1021/la0497447.

Boostani, S., Hosseini, S.M.H., Golmakani, M.T., et al., 2020. The influence of emulsion parameters on physical stability and rheological properties of Pickering emulsions stabilized by hordein nanoparticles. Food Hydrocoll. 101, 105520. https://doi.org/10.1016/j.foodhyd.2019.105520.

Cai, X., Zhai, J., Tran, N., Mulet, X., Drummond, C.J., 2022. Lipid nanoparticle steric stabilization roadmap. Adv. Biomembr. Lipid Self-Assembly 35, 41–75. https://doi.org/10.1016/bs.abl.2022.05.003.

Cain, J.D., Azizi, A., Maleski, K., et al., 2019. Sculpting liquids with two-dimensional materials: The assembly of $Ti_3C_2T_x$ MXene sheets at liquid–liquid interfaces. ACS Nano 13 (11), 12385–12392. https://doi.org/10.1021/acsnano.9b05088.

Cao, H., Escamilla, M., Anas, M., et al., 2021. Synthesis and electronic applications of particle-templated $Ti_3C_2T_z$ MXene–polymer films via Pickering emulsion polymerization. ACS Appl. Mater. Interfaces 13 (43), 51556–51566. https://doi.org/10.1021/acsami.1c16234.

Creighton, M.A., Ohata, Y., Miyawaki, J., Bose, A., Hurt, R.H., 2014. Two-dimensional materials as emulsion stabilizers: Interfacial thermodynamics and molecular barrier properties. Langmuir 30 (13), 3687–3696. https://doi.org/10.1021/la500216n.

Cui, S., McClements, D.J., He, X., et al., 2024. Interfacial properties and structure of Pickering emulsions co-stabilized by different charge emulsifiers and zein nanoparticles. Food Hydrocoll. 146, 109285. https://doi.org/10.1016/j.foodhyd.2023.109285.

de Carvalho-Guimarães, F.B., Correa, K.L., de Souza, T.P., et al., 2022. A review of Pickering emulsions: Perspectives and applications. Pharmaceuticals 15 (11), 1413. https://doi.org/10.3390/ph15111413.

Fan, Q., Yi, M., Chai, C., et al., 2022. Oxidation stability enhanced MXene-based porous materials derived from water-in-ionic liquid Pickering emulsions for wearable piezoresistive sensor and oil/water separation applications. J. Colloid Interface Sci. 618, 311–321. https://doi.org/10.1016/j.jcis.2022.03.073.

Feng, X., Dai, H., Ma, L., et al., 2020. Properties of Pickering emulsion stabilized by food-grade gelatin nanoparticles: Influence of the nanoparticles concentration. Colloids Surf. B Biointerfaces 196, 111294. https://doi.org/10.1016/j.colsurfb.2020.111294.

Fereidooni Moghadam, T., Azizian, S., 2014. Effect of ZnO nanoparticle and hexadecyltrimethylammonium bromide on the dynamic and equilibrium oil–water interfacial tension. J. Phys. Chem. B 118 (6), 1527–1534. https://doi.org/10.1021/jp4106986.

Fereidooni Moghadam, T., Azizian, S., Wettig, S., 2015. Synergistic behaviour of ZnO nanoparticles and gemini surfactants on the dynamic and equilibrium oil/water interfacial tension. Phys. Chem. Chem. Phys. 17 (11), 7122–7129. https://doi.org/10.1039/c5cp00510h.

Frigaard, I.A., Paso, K.G., de Souza Mendes, P.R., 2017. Bingham's model in the oil and gas industry. Rheol. Acta 56 (3), 259–282. https://doi.org/10.1007/s00397-017-0999-y.

Gao, Y., Wu, X., Qi, C., 2020. Janus-like single-chain polymer nanoparticles as two-in-one emulsifiers for aqueous and nonaqueous Pickering emulsions. Langmuir 36 (39), 11467–11476. https://doi.org/10.1021/acs.langmuir.0c01756.

Gazem, A., Krishna, S., Al-Yaseri, A., 2025a. Low-salinity enhanced oil recovery using biosurfactant-ZnO nanoparticle-xanthan gum formulations: A comparative study of rhamnolipid and sophorolipid systems. J. Mol. Liq. 432, 127894. https://doi.org/10.1016/j.molliq.2025.127894.

Gazem, A., Krishna, S., Al-Yaseri, A., 2025b. Polymer formulations with binary biosurfactants and zinc oxide nanoparticles for enhanced oil recovery. Fuel 400, 135733. https://doi.org/10.1016/j.fuel.2025.135733.

Ghaffarkhah, A., Hashemi, S.A., Isari, A.A., et al., 2024. Chemistry, applications, and future prospects of structured liquids. Chem. Soc. Rev. 53 (19), 9652–9717. https://doi.org/10.1039/d4cs00549j.

Gong, K., Yin, L., Pan, H., et al., 2022. Novel exploration of the flame retardant potential of bimetallic MXene in epoxy composites. Composites, Part B 237, 109862. https://doi.org/10.1016/j.compositesb.2022.109862.

Gonzalez Ortiz, D., Pochat-Bohatier, C., Cambedouzou, J., Bechelany, M., Miele, P., 2019. Pickering emulsions stabilized with two-dimensional (2D) materials: A comparative study. Colloids Surf. A Physicochem. Eng. Asp. 563, 183–192. https://doi.org/10.1016/j.colsurfa.2018.12.008.

Goodarzi, F., Zendehboudi, S., 2019. A comprehensive review on emulsions and emulsion stability in chemical and energy industries. Can. J. Chem. Eng. 97 (1), 281–309. https://doi.org/10.1002/cjce.23336.

Habib, S.H., Yunus, R., Zakaria, R., et al., 2024. Chemical enhanced oil recovery: Synergetic mechanism of alkali, surfactant and polymer with overview of methyl ester sulfonate as a green alternative for EOR surfactant. Fuel 363, 130957. https://doi.org/10.1016/j.fuel.2024.130957.

Han, R., Ma, X., Xie, Y., Teng, D., Zhang, S., 2017. Preparation of a new 2D MXene/PES composite membrane with excellent hydrophilicity and high flux. RSC Adv. 7, 56204–56210. https://doi.org/10.1039/c7ra10318b.

Hatchell, D., Song, W., Daigle, H., 2022. Effect of interparticle forces on the stability and droplet diameter of Pickering emulsions stabilized by PEG-coated silica nanoparticles. J. Colloid Interface Sci. 626, 824–835. https://doi.org/10.1016/j.jcis.2022.07.004.

He, L., Wang, L., Yang, L., et al., 2024. Functionalized $Ti_3C_2T_x$ MXene nanosheets for increased emulsion viscosity and enhanced heavy oil recovery. ACS Appl. Nano Mater. 7 (12), 14769–14779. https://doi.org/10.1021/acsanm.4c02462.

Hong, I.K., Kim, S.I., Lee, S.B., 2018. Effects of HLB value on oil-in-water emulsions: Droplet size, rheological behavior, zeta potential, and creaming index. J. Ind. Eng. Chem. 67, 123–131. https://doi.org/10.1016/j.jiec.2018.06.022.

Husin, H., Ariffin, T.S.T., Yahya, E., 2018. Rheological behaviour of water-in-light crude oil emulsion. IOP Conf. Ser. Mater. Sci. Eng. 358, 012067. https://doi.org/10.1088/1757-899x/358/1/012067.

Ibrahim Youssif, M., Saleh, S.M., 2024. A macro and micro-investigation of nanotechnology for enhanced oil recovery: A comprehensive review. J. Mol. Liq. 407, 125284. https://doi.org/10.1016/j.molliq.2024.125284.

Iravani, M., Khalilnezhad, Z., Khalilnezhad, A., 2023. A review on application of nanoparticles for EOR purposes: History and current challenges. J. Pet. Explor. Prod. Technol. 13 (4), 959–994. https://doi.org/10.1007/s13202-022-01606-x.

Jia, H., Dai, J., Wang, T., et al., 2022. The construction of pseudo-Janus silica/surfactant assembly and their application to stabilize Pickering emulsions and enhance oil recovery. Front. Chem. Sci. Eng. 16 (7), 1101–1113. https://doi.org/10.1007/s11705-021-2095-1.

Jiang, X., Liu, M., Li, X., Wang, L., Liang, S., Guo, X., 2021. Effects of surfactant and hydrophobic nanoparticles on the crude oil–water interfacial tension. Energies 14 (19), 6234. https://doi.org/10.3390/en14196234.

Jing, D., Song, D., 2017. Optical properties of nanofluids considering particle size distribution: Experimental and theoretical investigations. Renew. Sustain. Energy Rev. 78, 452–465. https://doi.org/10.1016/j.rser.2017.04.084.

Kalashnikova, I., Bizot, H., Bertoncini, P., Cathala, B., Capron, I., 2012. Cellulosic nanorods of various aspect ratios for oil in water Pickering emulsions. Soft Matter 9 (3), 952–959. https://doi.org/10.1039/c2sm26472b.

Kaushik, A., Joshi, D., Kumar Saw, R., Bala Rathi, K., Mitra, S., Mandal, A., 2024. Formation and characterization of nanoparticle assisted surfactant stabilized oil-in-water nanoemulsions for application in enhanced oil recovery. Fuel 359, 130500. https://doi.org/10.1016/j.fuel.2023.130500.

Kedar, V., Bhagwat, S.S., 2018. Effect of polar head surfactants on the demulsification of crude oil. Petrol. Sci. Technol. 36 (2), 91–98. https://doi.org/10.1080/10916466.2017.1405027.

Khezerloo-ye Aghdam, S., Kazemi, A., Ahmadi, M., 2024. Studying the effect of surfactant assisted low-salinity water flooding on clay-rich sandstones. Petroleum 10 (2), 306–318. https://doi.org/10.1016/j.petlm.2023.09.006.

Koh, A.Y.C., Prestidge, C., Ametov, I., Saunders, B.R., 2002. Temperature-induced gelation of emulsions stabilised by responsive copolymers: A rheological study. Phys. Chem. Chem. Phys. 4 (1), 96–102. https://doi.org/10.1039/b105990b.

Kolotova, D.S., Kuchina, Y.A., Petrova, L.A., Voron'ko, N.G., Derkach, S.R., 2018. Rheology of water-in-crude oil emulsions: Influence of concentration and temperature. Colloids Interfaces 2 (4), 64. https://doi.org/10.3390/colloids2040064.

Kondaraju, S., Farhat, H., Lee, J.S., 2012. Study of aggregational characteristics of emulsions on their rheological properties using the lattice Boltzmann approach. Soft Matter 8 (5), 1374–1384. https://doi.org/10.1039/c1sm06193c.

Kour, P., Shaheen, A., Tak, U.N., Gani, A., Qadri, H.K., Dar, A.A., 2024. Pickering emulsions of zein nanoparticles co-stabilized by Tween 20: An effective strategy to stabilize citral in low pH environment. Colloids Surf. A. 701, 134876. https://doi.org/10.1016/j.colsurfa.2024.134876.

Kumar, G., Behera, U.S., Mani, E., Sangwai, J.S., 2022. Engineering the wettability alteration of sandstone using surfactant-assisted functional silica nanofluids in

low-salinity seawater for enhanced oil recovery. J. Am. Chem. Soc. Eng. Au 2, 421–435. https://doi.org/10.1021/acsengineeringau.2c00007.
Kumar, N., Gaur, T., Mandal, A., 2017. Characterization of SPN Pickering emulsions for application in enhanced oil recovery. J. Ind. Eng. Chem. 54, 304–315. https://doi.org/10.1016/j.jiec.2017.06.005.
Kumar, N., Mandal, A., 2018a. Oil-in-water nanoemulsion stabilized by polymeric surfactant: Characterization and properties evaluation for enhanced oil recovery. Eur. Polym. J. 109, 265–276. https://doi.org/10.1016/j.eurpolymj.2018.09.058.
Kumar, N., Mandal, A., 2018b. Surfactant stabilized oil-in-water nanoemulsion: Stability, interfacial tension, and rheology study for enhanced oil recovery application. Energy Fuel. 32 (6), 6452–6466. https://doi.org/10.1021/acs.energyfuels.8b00043.
Li, F., Li, X., Huang, K., Luo, Y., Mei, X., 2021. Preparation and characterization of Pickering emulsion stabilized by hordein-chitosan complex particles. J. Food Eng. 292, 110275. https://doi.org/10.1016/j.jfoodeng.2020.110275.
Li, M., Yu, H., Gantumur, M.A., Guo, L., Lian, L., Wang, B., et al., 2024. Insight into oil-water interfacial adsorption of protein particles towards regulating Pickering emulsions: A review. Int. J. Biol. Macromol. 272, 132937. https://doi.org/10.1016/j.ijbiomac.2024.132937.
Liang, T., Hou, J.R., Qu, M., Xi, J.X., Raj, I., 2022. Application of nanomaterial for enhanced oil recovery. Pet. Sci. 19 (2), 882–899. https://doi.org/10.1016/j.petsci.2021.11.011.
Liu, J., Zhang, H., Sun, X., Fan, F., 2023. Development and characterization of Pickering emulsion stabilized by walnut protein isolate nanoparticles. Molecules 28 (14), 5434. https://doi.org/10.3390/molecules28145434.
Liu, L., Zhou, R., Chen, F., Wang, Z., Fan, Y., 2024. Facile preparation of redispersible/amphoteric nanochitin powder *via* choline chloride/propanedioic composite for stabilizing Pickering emulsions. Int. J. Biol. Macromol. 256, 128474. https://doi.org/10.1016/j.ijbiomac.2023.128474.
Lu, Y., Zhang, Y., Zhang, R., Gao, Y., Miao, S., Mao, L., 2024. Different interfaces for stabilizing liquid–liquid, liquid–gel and gel–gel emulsions: Design, comparison, and challenges. Food Res. Int. 187, 114435. https://doi.org/10.1016/j.foodres.2024.114435.
Lupu, A., Rosca, I., Gradinaru, V.R., Bercea, M., 2023. Temperature induced gelation and antimicrobial properties of pluronic F127 based systems. Polymers 15 (2), 355. https://doi.org/10.3390/polym15020355.
Ma, J., An, C.-X., Ma, L., Chen, Z., Zhang, W., Zhang, L., 2024. Amphiphilic MXene prepared by annealing or chemical modification for Pickering emulsion stabilization. SSRN. https://doi.org/10.2139/ssrn.5077781.
Maurya, N.K., Mandal, A., 2018. Investigation of synergistic effect of nanoparticle and surfactant in macro emulsion based EOR application in oil reservoirs. Chem. Eng. Res. Des. 132, 370–384. https://doi.org/10.1016/j.cherd.2018.01.049.
Ming, L., Wu, H., Liu, A., Naeem, A., Dong, Z., Fan, Q., et al., 2023. Evolution and critical roles of particle properties in Pickering emulsion: A review. J. Mol. Liq. 388, 122775. https://doi.org/10.1016/j.molliq.2023.122775.
Mishchuk, N.A., Sanfeld, A., Steinchen, A., 2004. Interparticle interactions in concentrate water–oil emulsions. Adv. Colloid Interface Sci. 112 (1–3), 129–157.
Murasiewicz, H., Illienko, K., 2024. Liquid-liquid two-phase system stabilized by Tween 40 and 80 surfactants: Multiparametric study. Pol. J. Chem. Technol. 26 (1). https://doi.org/10.2478/pjct-2024-0006.
Natalya, S.A.C., Kadja, G.T.M., Azhari, N.J., Khalil, M., Fajar, A.T.N., 2022. Two-dimensional (2D) nanomaterials for enhanced oil recovery (EOR): A review. FlatChem 34, 100383. https://doi.org/10.1016/j.flatc.2022.100383.
Narayan, S., Moravec, D.B., Hauser, B.G., Dallas, A.J., Dutcher, C.S., 2018. Removing water from diesel fuel: Understanding the impact of droplet size on dynamic interfacial tension of water-in-fuel emulsions. Energy Fuel. 32 (7), 7326–7337. https://doi.org/10.1021/acs.energyfuels.8b00502.
Niraula, B., King, T.C., Chun, T.K., Misran, M., 2004. Rheology properties of glucopyranoside-stabilized oil-water emulsions: Effect of alkyl chain length and bulk concentration of the surfactant. Colloids Surf. A Physicochem. Eng. Asp. 251 (1–3), 117–132. https://doi.org/10.1016/j.colsurfa.2004.08.071.
Pal, N., Mandal, A., 2020. Oil recovery mechanisms of Pickering nanoemulsions stabilized by surfactant-polymer-nanoparticle assemblies: A versatile surface energies' approach. Fuel 276, 118138. https://doi.org/10.1016/j.fuel.2020.118138.
Pal, R., 1993. Rheological behaviour of surfactant-flocculated water-in-oil emulsions. Colloids Surf. A Physicochem. Eng. Asp. 71 (2), 173–185. https://doi.org/10.1016/0927-7757(93)80342-C.
Pang, Y., Luo, Y., Li, Z., Luo, Y., Lou, H., Zhou, M., 2024. Pickering emulsion stabilized by lignin particles: Influence of oil phase, lignin concentration, and particle size. Colloid Polym. Sci. 302 (6), 901–909. https://doi.org/10.1007/s00396-024-05226-1.
Paola Marín Castaño, E., de Souza Mendes, P.R., Khalil De Oliveira, M.C., Tavares, F.W., Pérez Gramatges, P.A., da Silveira Carvalho, M., 2020. Linking the Rheology of W/O Crude Emulsions with the Droplet Aggregation Process. Available at: https://www.maxwell.vrac.puc-rio.br/51408/51408.pdf. (Accessed 30 September 2024).
Paryoto, S., Romdoni, Y., Kurnia, I., Muraza, O., Khalil, M., 2023. Synergy of surfactant mixtures and Fe_3O_4 nanoparticles for enhanced oil recovery (EOR). Inorg. Chem. Commun. 155, 111125. https://doi.org/10.1016/j.inoche.2023.111125.
Pei, H., Shu, Z., Zhang, G., Ge, J., Jiang, P., Qin, Y., Cao, X., 2018. Experimental study of nanoparticle and surfactant stabilized emulsion flooding to enhance heavy oil recovery. J. Pet. Sci. Eng. 163, 476–483. https://doi.org/10.1016/j.petrol.2018.01.025.
Pei, H., Zhao, J., Wu, Y., Liu, Y., Ning, C., Zhang, J., Zhang, G., 2024. Synergistic stabilization of emulsified solvent by nanobentonite and alkylethoxyglucoside to improve heavy oil recovery. Energy & Fuels 38 (13), 11616–11626. https://doi.org/10.1021/acs.energyfuels.4c01936.
Pinto, R.T., Feu, K.S., Dalmaschio, C.J., Nascimento, A., Lacerda, V., 2025. Oil recovery improvements based on Pickering emulsions stabilized by cellulose nanoparticles and their underlying mechanisms: A review. ACS Omega 10 (4), 3262. https://doi.org/10.1021/acsomega.4c08428.
Qazi, M.J., Schlegel, S.J., Backus, E.H.G., Bonn, M., Bonn, D., Shahidzadeh, N., 2020. Dynamic surface tension of surfactants in the presence of high salt concentrations. Langmuir 36 (27), 7956–7964. https://doi.org/10.1021/acs.langmuir.0c01211.
Qiu, F., Mamora, D., 2010. Experimental study of solvent-based emulsion injection to enhance heavy oil recovery in Alaska North slope area. In: SPE Can. Unconv. Resour. Int. Pet. Conf.. https://doi.org/10.2118/136758-MS.
Qu, M., Hou, J., Liang, T., Shao, Y., Raj, I., Yang, J., Xiao, L., 2020. Preparation and interfacial properties of ultralow concentrations of amphiphilic molybdenum disulfide nanosheets. Ind. Eng. Chem. Res. 59 (19), 9066–9075. https://doi.org/10.1021/acs.iecr.0c00217.
Qu, M., Hou, J., Liang, T., Qi, P., 2021. Amphiphilic rhamnolipid molybdenum disulfide nanosheets for oil recovery. ACS Appl. Nano Mater. 4 (3), 2963–2972. https://doi.org/10.1021/acsanm.1c00102.
Rao, M.A., 2014. Rheology of Fluid, Semisolid, and Solid Foods. Springer, New York. https://doi.org/10.1007/978-1-4614-9230-6.
Rasool, K., Helal, M., Ali, A., Ren, C.E., Gogotsi, Y., Mahmoud, K.A., 2016. Antibacterial activity of $Ti_3C_2T_x$ MXene. ACS Nano 10 (3), 3674–3684. https://doi.org/10.1021/acsnano.6b00181.
Rattanaudom, P., Alimin, A.A., Shiau, B.J. Ben, Harwell, J.H., Suriyapraphadilok, U., Charoensaeng, A., 2023. Experimental investigation of hydrophobic and hydrophilic silica nanoparticles on extended surfactant properties: Microemulsion, viscosity, and adsorption behaviors. Geoenergy Sci. Eng. 223, 211582. https://doi.org/10.1016/j.geoen.2023.211582.
Rezaei, A., Abdollahi, H., Derikvand, Z., Hemmati-Sarapardeh, A., Mosavi, A., Nabipour, N., 2020. Insights into the effects of pore size distribution on the flowing behavior of carbonate rocks: Linking a nano-based enhanced oil recovery method to rock typing. Nanomaterials 10 (5), 972. https://doi.org/10.3390/nano10050972.
Rezvani, H., Binks, B.P., Nguyen, D., 2024. Surfactant-nanoparticle formulations for enhanced oil recovery in calcite-rich rocks. Langmuir. https://doi.org/10.1021/acs.langmuir.4c03100.
Saha, R., Phukan, R., 2025. Enhanced oil recovery using chemical and nanoparticles for heavy oil sandstone reservoirs: Chemical vs nanofluid flooding. J. Mol. Liq. 431, 127707. https://doi.org/10.1016/j.molliq.2025.127707.
Salim, O., Mahmoud, K.A., Pant, K.K., Joshi, R.K., 2019. Introduction to MXenes: Synthesis and characteristics. Mater. Today Chem. 14, 100191. https://doi.org/10.1016/j.mtchem.2019.08.010.
Sastry, N.V., Dave, P.N., Valand, M.K., 1999. Dilute solution behaviour of polyacrylamides in aqueous media. Eur. Polym. J. 35 (3), 517–525. https://doi.org/10.1016/S0014-3057(98)00152-9.
Shah, S.N.A., Shahabuddin, S., Sabri, M.F.M., Salleh, M.F.M., Said, S.M., Khedher, K.M., Sridewi, N., 2020. Two-dimensional tungsten disulfide-based ethylene glycol nanofluids: Stability, thermal conductivity, and rheological properties. Nanomaterials 10 (7), 1340. https://doi.org/10.3390/nano10071340.
Sharma, T., Kumar, G.S., Chon, B.H., Sangwai, J.S., 2015. Thermal stability of oil-in-water Pickering emulsion in the presence of nanoparticle, surfactant, and polymer. J. Ind. Eng. Chem. 22, 324–334. https://doi.org/10.1016/j.jiec.2014.07.026.
Song, Y., Hou, Y., Ren, S., Qu, C., Li, M., Tu, Y., Wang, R., 2024. Pickering emulsion stabilized using modified gluten protein. J. Food Eng. 371, 111985. https://doi.org/10.1016/j.jfoodeng.2024.111985.
Srinivasan, S., Jothibas, M., Nesakumar, N., 2022. Enhancing electric double layer capacitance of two-dimensional titanium carbide (MXene) with facile synthesis and accentuated properties. Energy & Fuels. 36 (5), 2811–2820. https://doi.org/10.1021/acs.energyfuels.1c04092.
Sun, G.-Y., Zhang, H., Liu, D.-W., Li, C.-X., Yang, F., Yao, B., Duan, Z., Chen, X.-Y., Sheng, F.-J., 2022a. Co-adsorption behavior of aggregated asphaltenes and silica nanoparticles at oil/water interface and its effect on emulsion stability. Pet. Sci. https://doi.org/10.1016/j.petsci.2022.02.004.
Sun, Z., Yan, X., Xiao, Y., Hu, L., Eggersdorfer, M., Chen, D., Yang, Z., Weitz, D.A., 2022b. Pickering emulsions stabilized by colloidal surfactants: Role of solid particles. Particuology 64, 153–163. https://doi.org/10.1016/j.partic.2021.06.004.
Sunny, V., Muthukumaran, T., Philip, J., 2011. Temperature-induced gelation in dilute nanofluids. Langmuir 27 (20), 12361–12367. https://doi.org/10.1021/la202813a.
Szumała, P., Luty, N., 2016. Effect of different crystalline structures on W/O and O/W/O wax emulsion stability. Colloids Surf. A Physicochem. Eng. Asp. 499, 131–140. https://doi.org/10.1016/j.colsurfa.2016.04.022.

Taherpoor, P., Farzad, F., 2025. Exploring the synergistic effect of MXene@ZIF-8 hybrid composites for water treatment. Sci. Rep. 15 (1), 1–14. https://doi.org/10.1038/s41598-025-87527-1.
Thieme, J., Abend, S., Lagaly, G., 1999. Aggregation in Pickering emulsions. Colloid Polym. Sci. 277 (2–3), 257–260. https://doi.org/10.1007/pl00013752.
Thota, K., Sabapathy, M., Kakunuri, M., 2025. Candle soot/MXene incorporated robust superhydrophilic/underwater superoleophobic nanofibrous membrane for effective oil-in-water emulsion mixture separation. Colloids Surf. A Physicochem. Eng. Asp. 725, 137570. https://doi.org/10.1016/j.colsurfa.2025.137570.
Tliba, L., Edokali, M., Moore, T., et al., 2025. Spontaneous in-situ emulsification and enhanced oil recovery using functionalised silica nanoparticles: Insights from spontaneous imbibition and micromodel flooding tests. J. Mol. Liq. 424, 127021. https://doi.org/10.1016/j.molliq.2025.127021.
Wang, L., Shi, C., Pan, L., Zhang, X., Zou, J.J., 2020. Rational design, synthesis, adsorption principles and applications of metal oxide adsorbents: A review. Nanoscale 12 (8), 4790–4815. https://doi.org/10.1039/c9nr09274a.
Wang, S., Liu, Y., Liu, Y., Hu, W., 2023. Effect of HF etching on titanium carbide ($Ti_3C_2T_x$) microstructure and its capacitive properties. Chem. Eng. J. 452, 139512. https://doi.org/10.1016/j.cej.2022.139512.
Wang, W., Zhou, M., Xie, H., Dai, B., Lin, H., Han, S., 2025. MXene combined with β-cyclodextrin stabilized cottonseed oil Pickering emulsions for the preparation of nano-cutting fluids. Clean. Chem. Eng. 11, 100133. https://doi.org/10.1016/j.clce.2024.100133.
Wang, Y., Cui, Z., Feng, Y., Li, L., Zhang, Y., Guo, L., 2024. Effect of amphiphilic nanoparticles and non-ionic surfactants on emulsion stability. Tenside Surfactants Deterg. 62 (1), 27–36. https://doi.org/10.1515/tsd-2024-2617.
Xie, C., Lv, W., Wang, M., 2018. Shear-thinning or shear-thickening fluid for better EOR? —A direct pore-scale study. J. Pet. Sci. Eng. 161, 683–691. https://doi.org/10.1016/j.petrol.2017.11.049.
Xie, H., Zhao, W., Zhang, X., Wang, Z., 2022. Demulsification of bacteria-stabilized Pickering emulsions using modified silica nanoparticles. ACS Appl. Mater. Interfaces 14 (21), 24102–24112. https://doi.org/10.1021/acsami.2c02526.
Xu, F., Zhong, X., Li, Z., Cao, W., Yang, Y., Liu, M., 2022. Synergistic mechanisms between nanoparticles and surfactants: Insight into NP–surfactant interactions. Front. Energy Res. 10, 913360. https://doi.org/10.3389/fenrg.2022.913360.
Xu, G., Chang, J., Wu, H., Shao, W., Li, G., Hou, J., Kang, N., Yang, J., 2023. Enhanced oil recovery performance of surfactant-enhanced Janus SiO_2 nanofluid for high temperature and salinity reservoir. Colloids Surf. A Physicochem. Eng. Asp. 657, 130545. https://doi.org/10.1016/j.colsurfa.2022.130545.
Xu, K., Zhu, P., Colon, T., Huh, C., Balhoff, M., 2017. A microfluidic investigation of the synergistic effect of nanoparticles and surfactants in macro-emulsion-based enhanced oil recovery. SPE J. 22 (2), 459–469. https://doi.org/10.2118/179691-PA.
Xu, W., Zheng, S., Sun, H., Ning, Y., Jia, Y., Luo, D., Li, Y., Shah, B.R., 2021. Rheological behavior and microstructure of Pickering emulsions based on different concentrations of gliadin/sodium caseinate nanoparticles. Eur. Food Res. Technol. 247 (10), 2621–2633. https://doi.org/10.1007/s00217-021-03827-6.
Yadav, M., Kumar, M., Sharma, A., 2024. Review of $Ti_3C_2T_x$ MXene nanosheets and their applications. ACS Appl. Nano Mater. 7 (9), 9847–9867. https://doi.org/10.1021/acsanm.4c00316.
Yan, C., Altunbas, A., Yucel, T., Nagarkar, R.P., Schneider, J.P., Pochan, D.J., 2010. Injectable solid hydrogel: Mechanism of shear-thinning and immediate recovery of injectable β-hairpin peptide hydrogels. Soft Matter 6 (20), 5143–5156. https://doi.org/10.1039/c0sm00642d.
Yan, S., Cao, C., He, J., He, L., Qu, Z., 2019. Investigation on the electromagnetic and broadband microwave absorption properties of Ti_3C_2 MXene/flaky carbonyl iron composites. J. Mater. Sci. Mater. Electron. 30 (7), 6537–6543. https://doi.org/10.1007/s10854-019-00959-0.
Yang, G., Li, Y., Ma, L., Li, Z., Wang, J., Yang, S., 2025a. MXene-enhanced PDMS aerogels: Leveraging a Pickering emulsion strategy for advanced sensing applications. Chem. Eng. J. 503, 158525. https://doi.org/10.1016/j.cej.2024.158525.
Yang, T., Zan, S., Li, B., Li, L., Zhang, X., 2024. Interfacial adsorption dynamics of solid lipid particles at oil/water interfaces through QCM-D technique. Food Hydrocoll. 148, 109431. https://doi.org/10.1016/j.foodhyd.2023.109431.
Yang, Y., Fang, Z., Chen, X., Zhang, W., Xie, Y., Chen, Y., Liu, Z., Yuan, W., 2017. An overview of Pickering emulsions: Solid-particle materials, classification, morphology, and applications. Front. Pharmacol. 8, 235054. https://doi.org/10.3389/fphar.2017.00287.
Yang, Z., Jiang, C., Xiang, Q., Wu, J., Li, J., Cao, Z., Xiao, F., 2025b. Probing the stability of emulsified asphalts: A dual analysis of zeta potential and particle size. Fuel 396, 135266. https://doi.org/10.1016/j.fuel.2025.135266.
Yekeen, N., Padmanabhan, E., Syed, A.H., Sevoo, T., Kanesen, K., 2020. Synergistic influence of nanoparticles and surfactants on interfacial tension reduction, wettability alteration and stabilization of oil-in-water emulsion. J. Pet. Sci. Eng. 186, 106779. https://doi.org/10.1016/j.petrol.2019.106779.
Yu, S., Zhang, D., Jiang, J., Xia, W., 2019. Redox-responsive Pickering emulsions stabilized by silica nanoparticles and ferrocene surfactants at a very low concentration. ACS Sustain. Chem. Eng. 7 (19), 15904–15912. https://doi.org/10.1021/acssuschemeng.9b01881.
Zhang, L., Yu, Y., 2023. Improving the stability of water-in-oil emulsions with medium internal phase by the introduction of gelatin. Foods 12 (15), 2863. https://doi.org/10.3390/foods12152863.
Zhang, R., Yu, J., Liu, N., Gao, Y., Mao, L., 2022. W/O emulsions featuring ethylcellulose structuring in the water phase, interface and oil phase for multiple delivery. Carbohydr. Polym. 283, 119158. https://doi.org/10.1016/j.carbpol.2022.119158.
Zhang, T., Davidson, A., Bryant, S.L., Huh, C., 2010. Nanoparticle-stabilized emulsions for applications in enhanced oil recovery. In: SPE Symp. Improved Oil Recovery Proc. https://doi.org/10.2118/129885-MS.
Zhao, H., Yang, Y., Chen, Y., Li, J., Wang, L., Li, C., 2022. A review of multiple Pickering emulsions: Solid stabilization, preparation, particle effect, and application. Chem. Eng. Sci. 248, 117085. https://doi.org/10.1016/j.ces.2021.117085.
Zhao, M., Ma, Z., Song, X., Wu, W., Sun, Y., Cheng, Y., Wang, X., Yan, X., Dai, C., 2024a. Study on the main factors and mechanism of functional silica nanofluid spontaneous imbibition for enhanced oil recovery. J. Mol. Liq. 394, 123699. https://doi.org/10.1016/j.molliq.2023.123699.
Zhao, Q., Fan, L., Li, J., Zhong, S., 2024b. Pickering emulsions stabilized by biopolymer-based nanoparticles or hybrid particles for the development of food packaging films: A review. Food Hydrocoll. 146, 109185. https://doi.org/10.1016/j.foodhyd.2023.109185.
Zhao, S., Li, L., Zhang, H.B., Qian, B., Luo, J.Q., Deng, Z., Shi, S., Russell, T.P., Yu, Z.Z., 2020. Janus MXene nanosheets for macroscopic assemblies. Mater. Chem. Front. 4 (3), 910–917. https://doi.org/10.1039/c9qm00681h.
Zhou, B., Gao, S., Li, X., Liang, H., Li, S., 2020. Antioxidant Pickering emulsions stabilised by zein/tannic acid colloidal particles with low concentration. Int. J. Food Sci. Technol. 55 (5), 1924–1934. https://doi.org/10.1111/ijfs.14419.
Zhou, H., Wang, F., Wang, Y., Li, C., Shi, C., Liu, Y., Ling, Z., 2021. Study on contact angles and surface energy of MXene films. RSC Adv. 11 (10), 5512–5520. https://doi.org/10.1039/d0ra09125a.
Zhu, Y., Fu, T., Liu, K., Lin, Q., Pei, X., Jiang, J., Cui, Z., Binks, B.P., 2017. Thermoresponsive Pickering emulsions stabilized by silica nanoparticles in combination with alkyl polyoxyethylene ether nonionic surfactant. Langmuir 33 (23), 5724–5733. https://doi.org/10.1021/acs.langmuir.7b00273.